

**SU “St. Kliment Ohridski”**  
**Faculty of Biology**  
**Department of Biochemistry**

SOFIA  
UNIVERSITY



ST. KLIMENT  
OHRIDSKI  
est. 1888

# **Organization and surface features of hBest1 protein in models of biological membranes**

## **AUTHOR SUMMARY**

**of habilitation thesis for the scientific degree**

**“Doctor habilitatus”**

**4.3. Biological Sciences (Molecular biology)**

**Prof. Dr. Jordan Atanassov Doumanov**

**Sofia, 2023**

This dissertation was discussed and directed for defense at an extended meeting of the departmental council of the Department of Biochemistry at the Faculty of Biology of Sofia University “St. Kliment Ohridski” (**protocol № 703 of 05.10.2023**). The dissertation contains 196 pages in total, 30 pages of which are appendices. The dissertation is illustrated with 69 figures, 3 tables and 294 references are cited.

The public defense will take place on: .....

**Scientific Jury:**

Acad. Prof. Dr. Habil. Roumen Pankov – SU “St. Kliment Ohridski”  
Prof. Dr. Habil. Rossitza Konakchieva – SU “St. Kliment Ohridski”  
Assoc. Prof. Dr. Ivanka Tsacheva – SU “St. Kliment Ohridski”  
Acad. Prof. Dr. Habil. Ivan Ivanov – IMB, BAS  
Prof. Dr. Habil. Diana Petkova – IBPhBME, BAS  
Prof. Dr. Albena Aleksandrova – NSA  
Prof. Dr. Ivaylo Dimitrov – IP, BAS

**Alternate members:**

Assoc. Prof. Dr. Detelin Stefanov – SU “St. Kliment Ohridski”  
Assoc. Prof. Dr. Anastas Gospodinov – IMB, BAS

**This dissertation work was supported by grants** from the Bulgarian National Science Fund:

1. № KP-06-N23/7, 18.12.2018
2. DDVU 02/10, 17.12.2010,

as well as Scientific infrastructure project "Cell technologies in biomedicine" NPKNI (Agreements DO1-154/2018, DO1-275/2019), Bulgarian Ministry of Education and Science,

and by grants from Science Fund of SU "St. Kliment Ohridski":

1. "Behavior of hBest1 in sphingomyelin monolayers with the participation of  $\text{Ca}^{2+}$ , Glu and GABA",
2. "Visualization of Langmuir-Blodgett films of bestrophin-1 protein" Science Fund of SU "St. Kliment Ohridski"
3. "Behavior of the bestrophin-1 protein in lipid monolayers".

## List of abbreviations

hBest1 – human bestrophin-1

POPC – 1-palmitoyl-2-oleoyl-sn-glycero-3-phosphocholine

SM, eggSM– Sphingomyelin

Chol - Cholesterol

RPE – Retinal Pigment Epithelium

Glu – Glutamate

GABA –  $\gamma$  - aminobutyric acid

ERG – electroretinogram

EOG - electroocoulogram

KpBest1 – bestrophin-1 from Klebsiella

cBest1 (chBest1) – bestrophin-1 from chicken

Ap – apical membrane

Bl – basolateral membrane

AFM – Atomic Force Microscopy

BAM – Brewster Angle Microscopy

TLC – Thin Layer Chromatography

TER – Transepithelial Resistance

SNAs – Spherical Nucleic Acids

## Introduction

The biochemical and molecular mechanisms of vision are remarkable for their perfection in converting light into nerve impulses and chemical work through the sequences of enzymatic reactions that occur in the eye. The eye receives and focuses light on the centrally located retina, which is made up of photoreceptors, bipolar, amacrine, horizontal, and ganglion cells. The retina transmits the relevant information from the light through the optic nerve to the midbrain and thalamus, where it is processed (as visual perception) and sent to the visual cortex. In the visual cortex, different information (about color, shape, size, movement) is combined, resulting in a sense of experience. In the outer part of the retina are the cells of the retinal pigment epithelium (RPE), which are furthest from the light entering the eye.

Human bestrophin-1 (hBest1) is a  $\text{Ca}^{2+}$ -dependent transmembrane protein that is expressed in the retinal pigment epithelium, and mutations in the BEST1 gene cause retinal degenerations collectively termed “bestrophinopathies”. The present thesis describes the results of a large number of genetic, biochemical, biophysical, physicochemical and molecular biological integrated studies, which are important for understanding the relationship between the structure and function of the hBest1 channel protein and its pathophysiological significance.

Here, we show and discuss the state-of-the-art knowledge and understanding of the surface organization of hBest1, its interactions with essential membrane lipids (such as POPC, SM, and Chol) in models of biological membranes, and its association with various microdomains (e.g., lipid rafts) in cell membranes. This knowledge is fundamental to understanding how the activity of hBest1 channel molecules is modulated and regulated in cells.

Large-scale cell culture studies on the sorting of hBest1 and its mutant forms are included, showing that at least three sorting signals as well as phosphorylation are crucial for proper targeting of hBest1 to the basolateral membrane. We have shown that the expression of hBest1 in cells leads to a change in lipid metabolism, and the localization of the protein in the plasma membrane causes its “fluidization” and a reduction in the size of the ordered regions in it. The detected partial association (~30%) of hBest1 with lipid rafts defines the main role of the different microdomains for the surface (self)organization and activity of the protein.

The newly established stable cell line MDCK II – hBest1, as well as the developed original scheme for the purification and isolation of hBest1, opened up enormous opportunities for us to study the hBest1 protein. We found that ~51% helical structural elements are involved in the secondary structure composition of hBest1, with the secondary structure changing significantly depending on the presence of  $\text{Ca}^{2+}$ . Through atomic force microscopy, we determined the topology and took the first pictures of hBest1, thanks to which we saw not only a different conformation of the protein, but also a different organization (dimerization, trimerization) on the surface of the Langmuir-Blodgett films.

The ability to obtain pure hBest1 allowed us to use it in tensiometric measurements with Langmuir monolayers and thereby determine the surface behavior

and interactions of protein molecules with raft (SM and Chol) and non-raft (POPC) lipids.

Considerable space is devoted to the construction of  $\pi/A$  isotherms under physiological and dynamic conditions of compression and decompression, which simulate the dynamics of molecules in cell membranes. We found that the thermodynamic and favorable miscibility of hBest1 with some lipid (SM) molecules is counterbalanced by phase separation with others (POPC), but cholesterol improves and stabilizes the miscibility between the components. The equilibration and stabilization of the miscibility/phase separation between hBest1 and the (non)raft lipids has a direct effect on the association and localization of the protein in the different microdomains, its conformation, surface organization and its functions.

Studies performed in cell culture and those showing the interactions of hBest1 with membrane lipids are a prerequisite in the search for opportunities to integrate hBest1 into nanodiscs, polymeric and/or bicontinuous nanoparticles, as well as the use of spherical nucleic acids (SNA) to be delivery systems in future therapies of bestrophinopathies.

## **I. Purpose and tasks**

The purpose of the thesis was to trace and investigate the role of hBest1 in the cell, its structure, organization and functions, the relationship between structure and functions, as well as the molecular mechanisms leading to bestrophinopathies. Studies of the structure and functional activity of hBest1 have been challenging because the protein is predominantly expressed in the basolateral plasma membrane of retinal epithelial cells that lose its translation *in vitro*.

To achieve the goal, the following tasks were set, divided into two directions:

1. Cell culture studies as model systems, which include: a) establishment of cell lines from hBest1 (normal and mutant forms) transfected eukaryotic cells; b) proving the expression of hBest1 proteins in them, their cellular localization in polar cells and their association with lipid rafts; c) determining the influence of hBest1 on cell development and their metabolism.

2. Studies with biological membrane models that are directly dependent on the isolation and purification of hBest1 from stably transfected MDCK II - hBest1 cells and include: a) determination of the surface physicochemical characteristics of Langmuir monolayers and Langmuir-Blodgett films of purified hBest1; b) determination of the surface physicochemical characteristics of two- and three-component Langmuir monolayers and Langmuir-Blodgett films containing hBest1 and combinations of the prevalent membrane lipids phosphatidylcholine, sphingomyelin and cholesterol. The descriptions of the methods used are in the thesis.

## II. Results and discussion

### 1. Studies of hBest1 in cell cultures as model systems

#### 1.1. Transient expression of hBest1 and its mutant forms in MDCK II cells

Our studies of hBest1 began by demonstrating its expression in various cell lines. The lack of endogenous translation of hBest1 in MDCK II, RPE-J, RPE-1, HeLa and HEK293 cell lines indicates that after transfection they can be used to study the protein without further silencing of endogenous transcription of the *BEST1* gene. Due to the impossibility to study the **sorting** of hBest1 in retinal cells from both RPE-J and RPE-1 lines, we focused on studying the behavior of the protein in cells from another line, namely - **MDCK II**. They are one of the most widely used models of polar epithelial cells. Polarization in these cells develops in only about five days of culture, there is no overlap of cells in monolayer formation, which determines the clear and easy distinction of BI- and Ap - domains using different marker proteins. Endogenous transcription of *BEST1* in cells of the MDCK II line showed the presence of the transcript, but at a very low level (after the 34th of 40 cycles when performing quantitative real-time PCR), which was about 40% lower than that observed in RPE-J cells (**Figure 1**). Similar to the cells described above, MDCK II cells did not synthesize the hBest1 protein, whereas cells transfected with human BEST1 expressed the Best1 protein of the expected size of 68 kDa (**Figure 1**). For these reasons, MDCK II cells were preferred by us to study the localization of normal/wild-type hBest1.

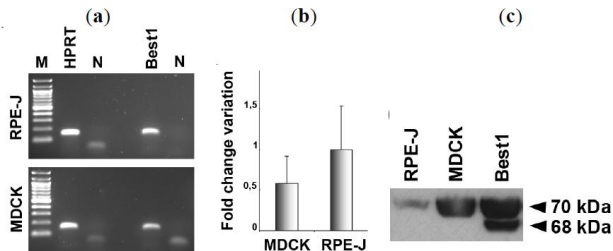


**Figure 1.** Endogenous expression of *BEST1* in MDCK cells. (a) *HPRT* and *BEST1* mRNAs are expressed in MDCK and RPE-J cells. M–100 bp ladder, N–negative control; (b) Quantification of *BEST1* expression levels between MDCK and RPE-J cells using quantitative Real-Time PCR. Fold change variation in *BEST1* expression levels is reported as  $2^{-\Delta\Delta Ct}$  value, the reference mRNA being *HPRT* (mean  $\pm$  SEM., n = 2); (c) Western blot analysis - Best1 protein is not synthesized by RPE-J or MDCK cells. After transfection, MDCK produce human Best1 at 68 kDa. (Doumanov et al., 2013)\*.

**\* All research papers cited in the figures are original author's publications related to the dissertation topic.**

hBest1 is localized to the basolateral membrane of RPE as well as RPE-J cells. To determine whether this sorting was similar in MDCK II cells, we transiently

transfected with a construct containing the normal human *BEST1* gene. All cells showed the typical morphology characteristic of polarized cells. Only in transfected cells, confocal sections showed basolateral localization of hBest1 below the plane where ZO-1 resides, as well as basolateral colocalization with  $\beta$ -catenin, indicating the membranes that separate neighboring cells as well as their basolateral surfaces (**Figure 2**).

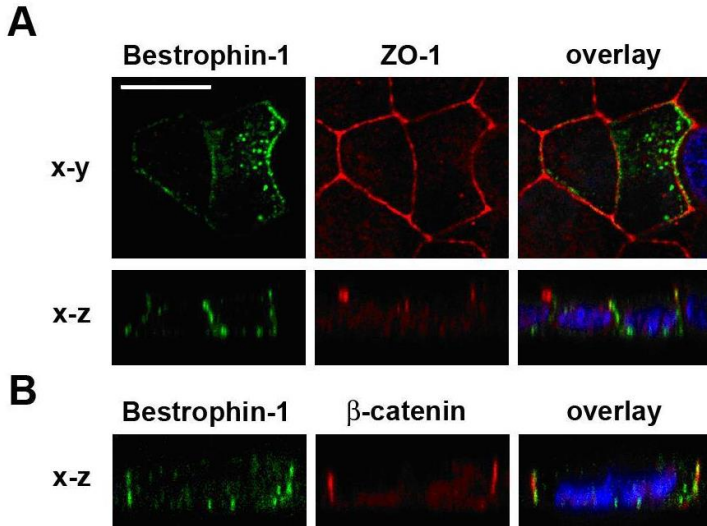


**Figure 2.** Basolateral localization of hBest1 in MDCK II cells. **(A)** Transfected MDCK cells express hBest1 (green) at the basolateral surface, colocalizing with the tight-junction marker ZO-1 (red) on X-Y and X-Z single confocal scans; **(B)** hBest1 (green) at the basolateral surface, colocalizing with the basolateral marker  $\beta$ -catenin (red) on X-Z single scan. Nuclei are in blue, scale bar = 10  $\mu$ m (**Doumanov et al., 2013**).

Quantitative analysis of basolateral and apical fluorescence signals showed similar membrane distribution of hBest1 and  $\beta$ -catenin molecules, respectively 90% and 91% of both proteins are preferentially localized on the basolateral membrane of cells. A number of membrane proteins (including ion channels) in the RPE show an inverted localization (reversed polarity) compared to their sorting in other epithelial cells.

Our data show that MDCK II cells after transfection can express and process the hBest1 protein. The basolateral localization of the protein is similar to that in retinal cells, suggesting that both cell types interpret the sorting signals in the hBest1 molecule in a **similar** manner.

By site-specific mutagenesis, we generated **hBest1 mutants** and analyzed their synthesis and localization in transiently transfected MDCK II cells. Mutations in the constructs were located in different domains of the protein, in **putative basolateral tyrosine and dileucine sorting motifs** (p.Y85VTL, p.Y97ENL, p.L206L207, p.Y227DWI). These mutations occur in BVMD patients (p.R25W, p.Y85H, p.L100R,

p.L207I, p.Y227N), including the newly described (at that time, 2009) p.Q96R mutation, which is adjacent with the Y97ENL motif. To investigate whether these mutations affect the sorting and localization of hBest1, we analyzed the polarized expression of the different mutant forms in MDCK II cells. Cell polarization was established by the formation of tight junctions between neighboring cells, fluorescently and confocally visualized by ZO-1, while localization of the mutants was determined by co-localization with the basolateral marker  $\beta$ -catenin (**Figure 3**).

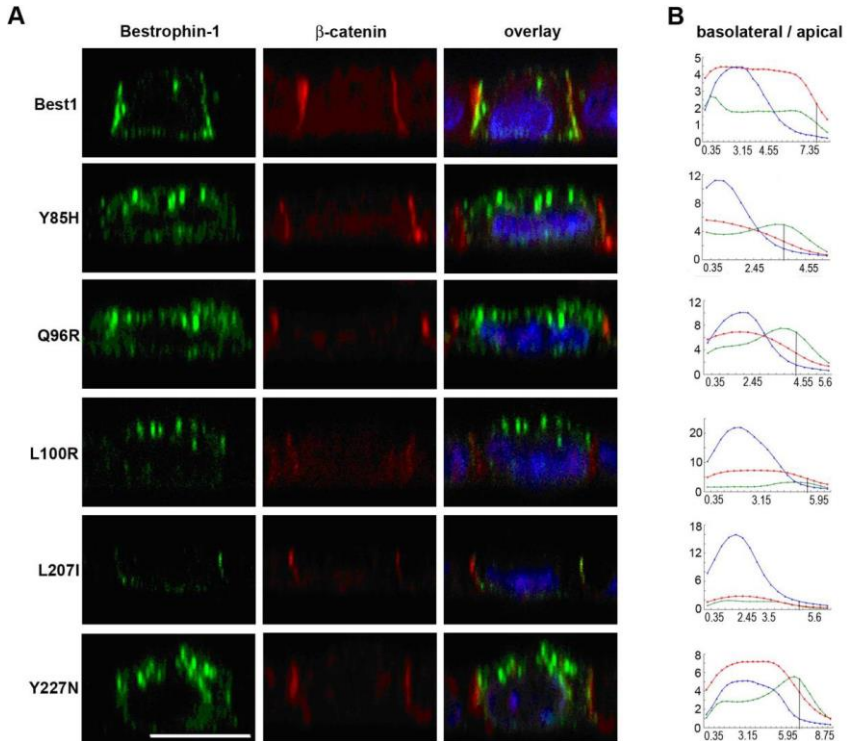


**Figure 3.** Mutations in potential sorting motifs affect the basolateral localization of hBest1 in polarized MDCK II cells. **(A)** X-Z confocal single image scan of transiently transfected cells with different *BEST1* cDNA constructs showing mislocalization of mutants Y85H, Q96R, L100R and Y227N. Cells were stained for hBest1 (green),  $\beta$ -catenin (red) and nuclei (blue). Scale bar = 10  $\mu$ m; **(B)** Z-series confocal stack signals corresponding to each labeling were quantified. Curves indicate the pixel intensity of each section along the Z-axis for each cell (hBest1, green;  $\beta$ -catenin, red; nuclei, blue). The black vertical line indicates the Z-focal plane chosen as threshold for apical and basolateral domains separation. Basolateral and apical sides are as indicated. Horizontal axis represents  $\mu$ m distance and vertical axis shows pixel intensities (**Doumanov et al., 2013**).

Protein molecules carrying the mutations p.Y85H, p.Q96R, p.L100R and p.Y227N showed impaired localization and increased apical expression (**increased**

green fluorescence signal above the level of  $\beta$ -catenin in the X-Z plane) in cells compared to non- mutant molecules. Only for p.L207I cell distribution was basolateral and a co-localization with the  $\beta$ -catenin red signal was observed, similar to that of normal hBest1 (**Figure 3**). The signal intensity values at each Z-focal plane in a single cell show a different shape of the curves for the mutant proteins compared to the values for both  $\beta$ -catenin and normal hBest1. The maximum signal intensity for the mutant forms was shifted to the apical part of the curves, corresponding to increased apical staining in the cells (**Figure 3**). Quantitative analysis of hBest1 distribution between Ap and Bl membranes showed increased targeting of the protein to the apical membrane by 15% for p.Y85H ( $p = 5.37 \times 10^{-5}$ ), 10% for p.Q96R ( $p = 0.0001$ ), 6% for p.L100R ( $p = 0.0009$ ) and 9% for p.Y227N ( $p = 5.20 \times 10^{-5}$ ), while the p.L207I mutant showed no change in its basolateral localization (**Figure 4**).

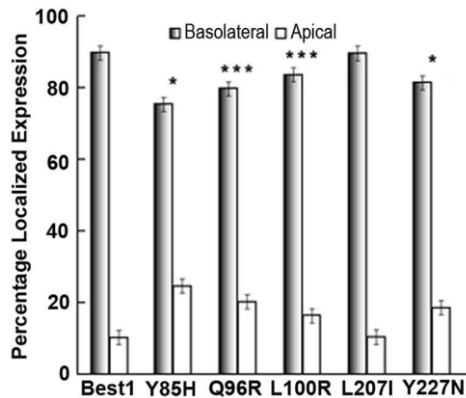


**Figure 4.** Bar graph illustrating quantification of hBest1 mutants distribution in the basolateral and apical domains of the cells compared with normal protein (mean  $\pm$  SEM,  $n = 10$ , \*  $p < 0.01$ , \*\*\*  $p < 0.0001$ ) (**Doumanov et al., 2013**).

The unaltered basolateral localization of the p.L207I mutant indicates that the putative sorting motif L206L207, which is located in the large cytoplasmic domain of hBest1, may not be required for basolateral localization. It is possible, however, that due to the similar structure of amino acids L and I, cell sorters do not distinguish between them, recognize them in the same way and direct the proteins basolaterally. Therefore, the pathogenic mechanism of this mutation is most likely not related to changes in hBest1 sorting.

For the mutants p.Y85H and p.Q96R, which showed the greatest changes in their localization compared to the wild-type protein, colocalization analysis was performed with ZO-1 and WGA (wheat germ agglutinin) as an extracellular apical marker. The two protein mutants partially localized above tight junctions in cells and partially colocalized with WGA at the apical membrane, which was not observed with normal hBest1. Furthermore, after biotinylation of p.Y85H and p.Q96R at the apical

and basolateral membranes, the increased apical localization of both mutant forms of the protein was reconfirmed. In addition to sorting, the p.Y85H mutation, which is located in the second transmembrane domain of hBest1, is important for both the correct topology and ion permeability of the protein, due to the replacement of a hydrophobic with a positively charged amino acid.

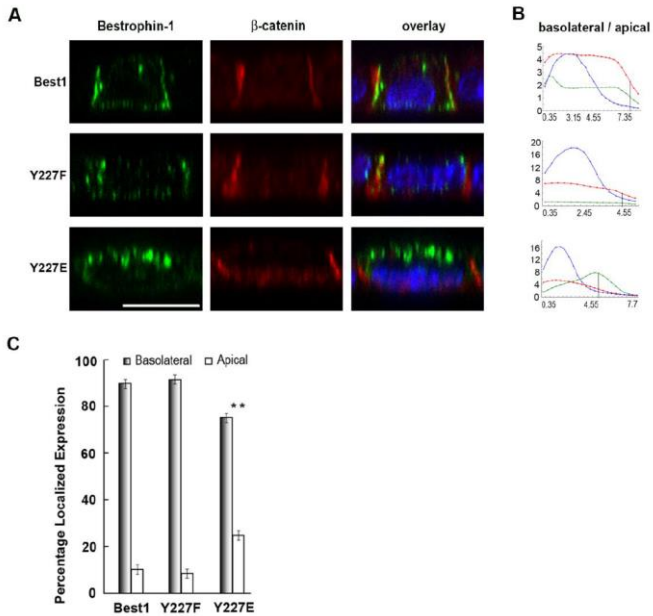


**Figure 5.** Correct basolateral sorting requires that the tyrosine at position 227 is not phosphorylated. **(a)** X-Z confocal single scan showing that constitutively phosphorylated hBest1 (Y227E) is partially targeted to the apical membrane compared to normal and non-phosphorylated (Y227F) Best1. Best1 in green,  $\beta$ -catenin in red, nuclei in blue. Scale bar = 10  $\mu$ m; **(b)** Quantification of basolateral to apical localization of the three markers (hBest1, green;  $\beta$ -catenin, red; nuclei, blue) along the Z-axis confirming the result. Vertical line indicated basolateral-apical domains separation. Horizontal axis represents  $\mu$ m distance and vertical axis shows pixel intensities; **(c)** Bar graph of the repartition percentage of hBest1 between basolateral and apical domains (mean  $\pm$  SEM,  $n = 10$ , \*\*  $p < 0.005$ ). (Doumanov et al., 2013).

In 2005, Mullins and colleagues reported a patient with BVMD in whom an increased amount of hBest1 was observed on histological sections of the eye along the apical membrane of the RPE. The patient carries a Y227N mutation, suggesting a possible role of the p.Y227DWI motif in the proper targeting and function of the protein (this mutation also affects the ion permeability, which is only 28% of that of the normal protein). We also confirmed that the p.Y227N mutation leads to increased Ap expression of these proteins (see above) and that the Tyr at position 227 (Y227) is

important for BI targeting. hBest1 has already been found to be phosphorylated. Therefore, the question of whether Y227 phosphorylation affects protein localization was raised. Tyrosine 227 was replaced by glutamate and phenylalanine in two mutant forms of the protein, and these substitutions were designed to "simulate" phosphorylation (pseudophosphorylation) or block it. The results show that the pseudo-phosphorylated p.Y227E proteins increase in the apical membrane, whereas the non-phosphorylated p.Y227F forms retain basolateral staining similar to the normal hBest1 protein (**Figure 5**). These results suggest the important role of non-phosphorylated tyrosine for basolateral sorting, i.e. Y227 must be unphosphorylated to be recognized by the basolateral sorting machinery in the cell and for the protein to be properly localized to the membrane.

The last mutation we examined was R25W, which differs from the other mutant forms because it does not "lie" near a potential sorting tyrosine motif, but near potential sorting leucine motif composed of three residues of the amino acid leucine - L20LL. Apical expression of R25W mutants was 60% higher compared to normal proteins, indicating that this leucine motif is important for proper hBest1 sorting.

The basolateral sorting-impaired mutants studied showed between 60% and 150% increase in the amount of protein at the apical surface of the cells compared to normal hBest. A correlation was observed that the disturbances in the localization of the mutants were proportional to the distance of the mutation from the cell membrane - Y85H > Q96R-Y227N > L100R. It is likely that apical accumulation of the protein over time causes disruption of ion permeability in the apical and basolateral membranes of RPE cells. A decrease in the amount of hBest1 on the BI membrane may explain the decrease in the light peak of clinical electrooculograms in BVMD patients. The obtained results show that the impaired localization of the hBest1 mutants corresponds to disturbances in the composition and structure of the potential basolateral sorting motifs Y85VTL, Y97ENL and Y227DWI, which can be recognized by the "sorters" when they are located in the cytoplasmic part of the protein (like the tyrosine motifs Y97ENL and Y227DWI). The results of our studies showed the lack of a complete "reversal" of the localization of the mutant proteins upon disruption of the structure of the sorting motifs, so it is likely that several motifs are involved in sorting and have a **cumulative effect** on hBest1 localization. Furthermore, tyrosine phosphorylation is most likely part of the sorting process.

## 1.2. Stable expression of hBest1 in cells of the MDCK II cell line

MDCK II cells that were transiently transfected with hBest1 and its mutant forms lost protein expression about 72 h after transfection. For this reason, we set out to establish and characterize a stably transfected RPE-1 cell line (despite the disadvantages of these cells) expressing hBest1, which would aid in studying the function and structure of the protein in retinal epithelial cells. RPE-1 cells were stably transfected with hBest1, with relatively weak in intensity positive protein expression fluorescence signals detected in almost 100% of cells.

Obtaining stable retinal cells from the RPE-1 cell line expressing hBest1 approximates the phenotype of these cells to that of "native" RPE cells. Despite the

good results we obtained with the stably transfected cells, this cell line was not used in our further studies due to the low levels of hBest1 translation and the differences in growth characteristics with the non transfected cells. For these reasons, we set out to establish a **new line** of epithelial MDCK II cells stably expressing hBest1.

MDCK II cells were stably transfected with the hBest1 gene. Transfection efficiency was determined by immunofluorescence (**Figure 6**).

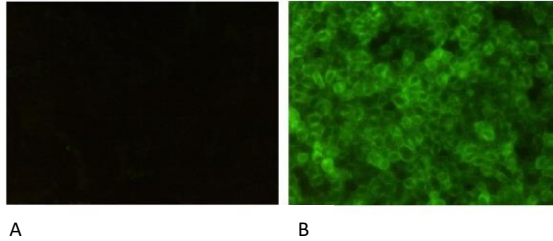


**Figure 6.** Immunofluorescence of untransfected and stably transfected with hBest1 MDCK II cells. **A)** MDCK II cells not transfected with hBest1 (control). No specific signal was observed for hBest1. **B)** MDCK II cells stably transfected with human hBest1. Expression of hBest1 (green color) was observed in almost all cells.

About 100% of the cells were positive for hBest1 expression. The observed signal intensity for hBest1 was strong and the signal was correctly localized along the cell membrane. The result was also confirmed biochemically by Western blot analysis, where a signal corresponding to the molecular mass of hBest1 (about 68 kDa) was detected in the transfected cells. Similar results were obtained even after several passages as well as after freezing/thawing the cells. Thus, we proved that hBest1 transfection was successful and the isolated and stabilized cells gave rise to the **new MDCK II - hBest1 cell line**.

After examining the growth characteristics of untransfected MDCK II and MDCK II - hBest1 cells, we found that hBest1 did **not change the growth curves** and did not affect cell growth. For both cell types, we observed similar cell population growth rates and no difference was observed in the time it took for them to go through the different growth phases. We also found close values of the mitotic index, which showed that **hBest1 also did not affect the rate of cell division**.

From the images taken, **no difference in morphology** was detected between the cells of the two lines (they showed a normal isodiametric shape) (**Figure 7**). These results, in contrast to the results obtained with transfected RPE-1 cells, indicate that MDCK II - hBest1 cells can be used in our subsequent studies.

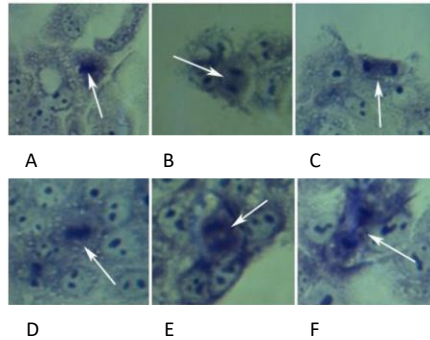


**Figure 7.** MDCK II and MDCK II - hBest1 cells in different phases of mitosis. Untransfected cells: A) metaphase; B) anaphase; C) telophase. Stably transfected MDCK II - hBest1 cells: D) metaphase; E) anaphase; F) late telophase. Dividing cells in the respective phases are indicated by arrows.

### 1.2.1. Examination of hBest1 sorting in polarized MDCK II - hBest1 cells

To establish the cellular localization of hBest1 in stably transfected MDCK II cells, we compared the immunofluorescence signal of hBest1 to ZO-1 as well as to GM130. The results obtained show that hBest1 is localized along the basolateral membrane in MDCK II - hBest1 cells polarized for six days (**Figure 8**).

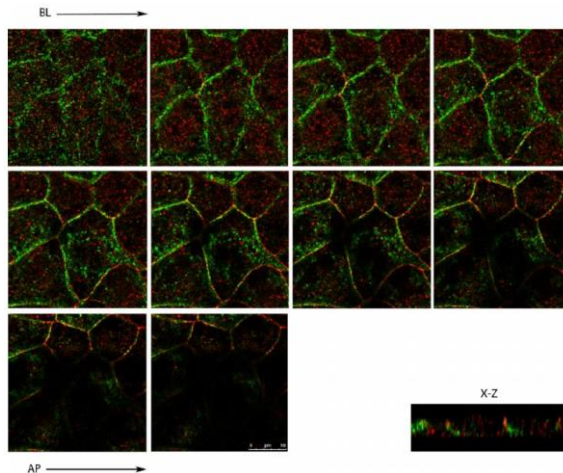


**Figure 8.** Confocal microscopy images of stably transfected MDCK II - hBest1 cells polarized for six days. Images show consecutive sections of cells in the basolateral (Bl) (top left) to apical (Ap) (bottom right) direction. The signal of hBest1 is in green and that of ZO-1 is in red. Bar = 10  $\mu$ m.

Control untransfected MDCK II cells were polarized for six days, showing a strong ZO-1 signal and no signal for endogenous hBest1 expression.

In addition to B1 protein targeting, we also found partial co-localization of hBest1 and GM130 signals, which is likely due to hBest1 protein molecules still "moving" along the biosynthetic pathways of the cell (due to overexpression of the protein). From the results obtained, we can conclude that hBest1 does **not affect the polarization time** of MDCK II cells, since untransfected and stably transfected cells reach polarization at approximately the same time, and that sorting signals in MDCK II cells are "interpreted" as in retinal cells.

### 1.2.2. Study of transepithelial resistance in monolayers of MDCK II - hBest1 cells

Conducted cell resistance experiments in the process of polarization of transfected and non-transfected MDCK II cells showed close values of transmembrane resistance during the first days (first-fourth day) (**Figure 9**).

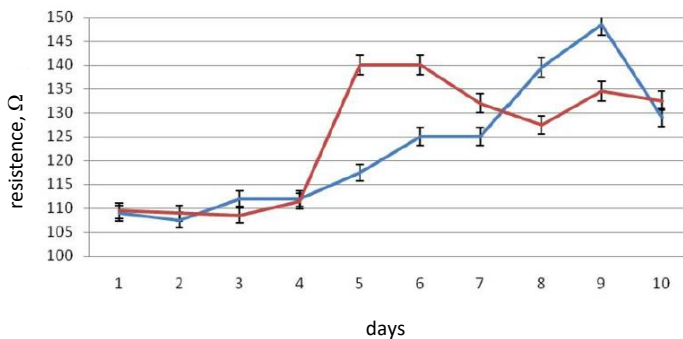


**Figure 9.** Transepithelial resistance of stably transfected (in blue) MDCK II - hBest1 and untransfected (in red) MDCK II cells for 10 days (**Mladenova et al., 2015a**).

From the fourth to the seventh day, lower transmembrane resistance values (115 - 125 Ω) were found in MDCK II - hBest1 cells compared to MDCK II cells (133 - 140 Ω). This can be explained by the presence of a large amount of hBest1 protein in the plasma membrane and the increased passage of ions into the extracellular space. From day seven to ten, transfected cells showed a higher transmembrane resistance (140 - 125 Ω) with values similar to those from day four to seven in MDCK II cells, the increase in TER probably being due to a decrease in the intracellular ion pool ( $\text{Cl}^-$ ) and reaching equilibrium in ion transport with the participation of hBest1. A similar balance in ion transport may also explain the decrease in TER in MDCK II cells after their polarization.

The reduction in resistance in MDCK II - hBest1 cells may also be due to incompletely formed or changes in tight junctions to be influenced by hBest1, through calcium ions "acting" on the actin cytoskeleton. The increased ion conductance due to

the action of hBest1, as well as its possible function as a regulator of calcium channels, may affect the "contractions" of actin (a similar reorganization of the actin cytoskeleton was found in transfected cells) to "pull " ZO -1 and the occluded ones located in the tight contacts. As a result, they will be slightly open, so the space formed between the tight junctions is enough for the passage of ions. Thus, TER may decrease until MDCK II - hBest1 cells reach ion transport equilibrium again. From the obtained results it follows that cell polarization is not always related to the adequate/synchronous increase in transepithelial resistance.

The amino acid Glu, GABA and ATP affect the functional activity of hBest1, therefore we would expect them to also affect the TER of the cell monolayer. In MDCK II - hBest1 cells, a faster reaching maximum TER (between 125 and 138  $\Omega$ ) was observed in all experimental settings (involving these components) on day 5-6, while in the control maximum TER (120  $\Omega$ ) was at Day 7 (Figure 10).

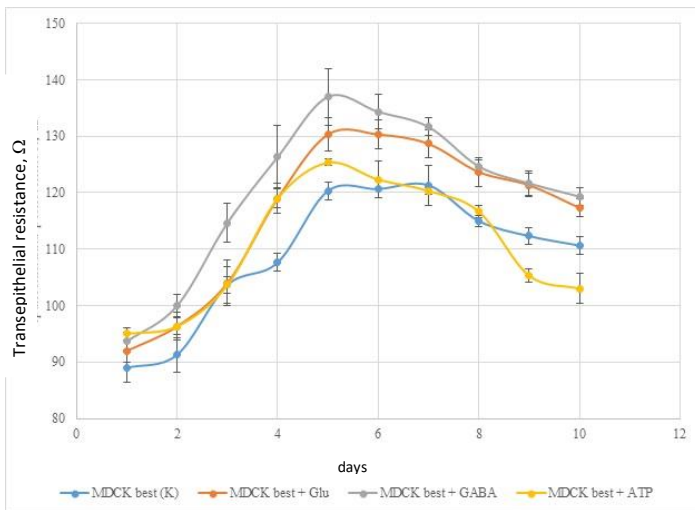


**Figure 10.** Change in TER in MDCK II - hBest1 cells incubated with ATP, Glu and GABA for 10 days. Results are presented as mean  $\pm$  SE, n = 3.

The high TER values obtained with the addition of Glu and GABA suggest a decrease in hBest1 activity and, accordingly, an increase in the resistance of the cell monolayer. This applies to a greater extent for GABA, since unlike MDCK II - hBest1, GABA treated non transfected cells in the last days of the measurement showed TER values close to the control series (about 95 – 100  $\Omega$ ). In contrast, in cells treated with ATP, we found the lowest TER values (about 100 – 102  $\Omega$ ) at the end of the experiment. This result is most likely due to the activation of hBest1 by binding to ATP and increasing the flow of ions through the cells of the monolayer. The inhibition and activation of hBest1 (indirectly indicated by TER) is not unexpected and is due to

increased concentrations of Glu, GABA (which hBest1 transports extracellularly across the membrane), and ATP in the culture medium.

Biological membranes are highly dynamic lamellar structures that are constantly reorganized and remodeled by cellular phospholipases. PLA<sub>2</sub> enzymes (EC 3.2.1.4) were found to be involved in the degradation of photoreceptor outer segments after their phagocytosis by the RPE. Therefore, to investigate the role of hBest1 in transepithelial resistance in cell membrane reorganization, hBest1 transfected and non transfected MDCK II cells forming a monolayer were subjected to the action of sPLA<sub>2</sub> at two stages of its development within ten days - at 100 % confluence (**Figure 11**) of the cells and at maximum TER of the monolayer (**Figure 12**).

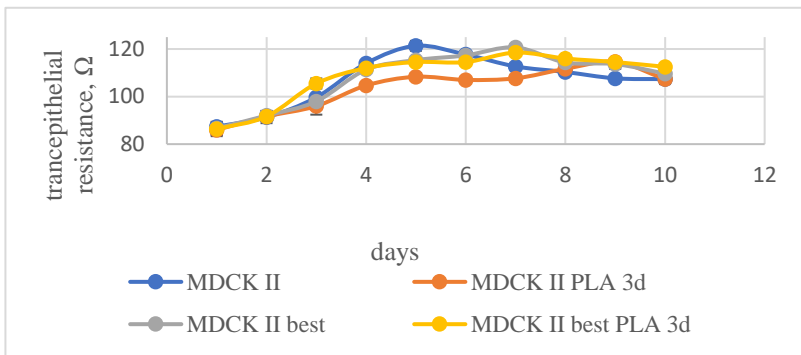


**Figure 11.** Change in TER (determined over 10 days) in MDCK II and MDCK II -hBest1 cells incubated with 2 $\mu$ M sPLA<sub>2</sub> for 15 min on the day of reaching 100% confluence (day 3). Results are presented as mean  $\pm$  SE, n = 3.

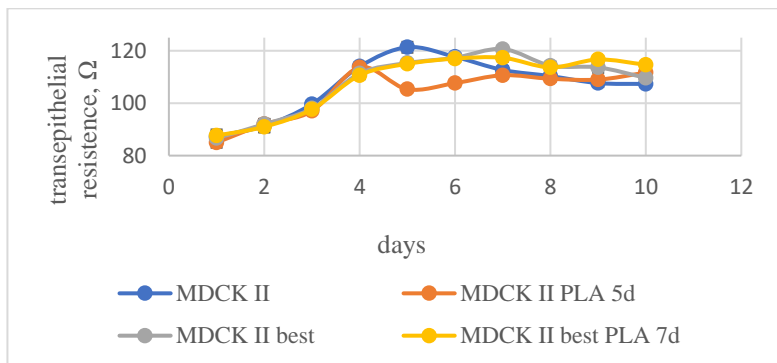


**Figure 12.** Change in TER (determined over 10 days) in MDCK II and MDCK II -hBest1 cells incubated with 2 $\mu$ M sPLA<sub>2</sub> for 15 min on the day of reaching TER<sub>max</sub>. Results are presented as mean  $\pm$  SE, n = 3.

We found a strong effect of sPLA<sub>2</sub> on untransfected cells and a decrease in TER (about 20%) in contrast to the TER of the monolayer of MDCK II - hBest1 cells, where minimal changes (below 10%) were observed (**Figures 11 and 12**). We observed a similar effect when tracing TER in a monolayer of untransfected cells for six hours after sPLA<sub>2</sub> treatment (**Figures 13 and 14**).

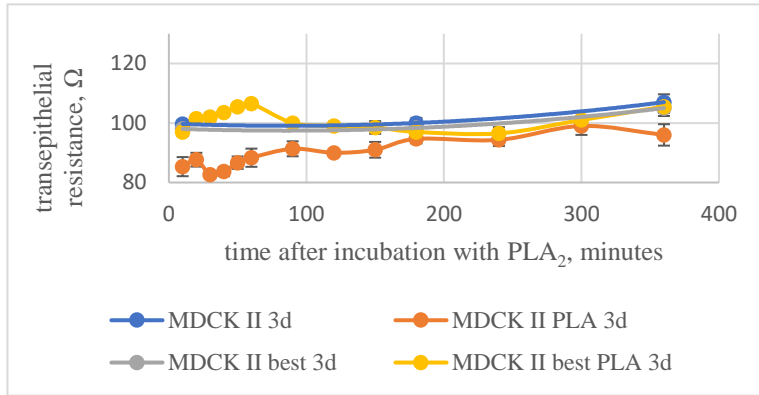


**Figure 13.** Change in TER (over 350 min) in MDCK II and MDCK II - hBest1 cells incubated with 2<sub>M</sub> sPLA<sub>2</sub> for 15 min on the day of reaching 100% confluence (day 3). Results are presented as mean ± SE, n = 3.

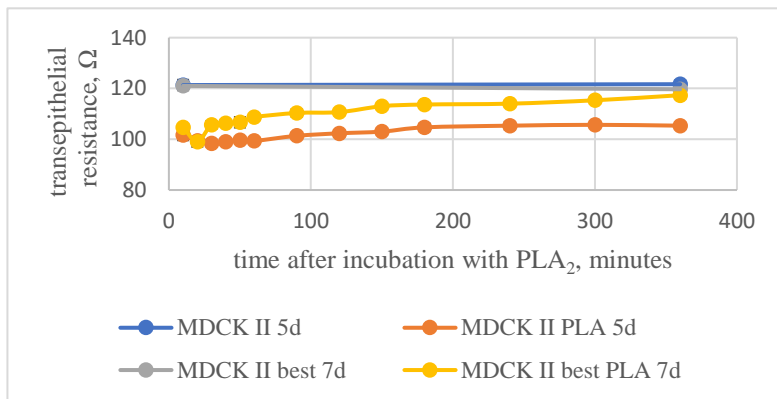


**Figure 14.** Change in TER (over 350 minutes) in MDCK II and MDCK II - hBest1 cells incubated with 2<sub>M</sub> sPLA<sub>2</sub> for 15 minutes on the day of reaching TER<sub>max</sub>. Results are presented as mean ± SE, n = 3.

This effect can be explained by an increase in ion permeability, due to disruption of the membranes caused by the enzymatic action of sPLA<sub>2</sub>, which recovers

over time. In MDCK II - hBest1 cells, however (**Figure 13**), the action of sPLA<sub>2</sub> had the opposite effect. TER increased (from 98 to 108  $\Omega$ ) for the first 60 minutes, then by the fourth hour the values decreased (to 98  $\Omega$ ) and at the end of the experiment reached those measured in the control cells (about 105  $\Omega$ ). The enzymatic action of sPLA<sub>2</sub> increases the liquid-ordered phase (which decreases permeability) and decreases the liquid-disordered phase in cell membranes. This change and reorganization in the phase states may lead to a change in the structure and function of hBest1 and inhibition of its channel functions, which may be related to the increase in TER.

### **1.2.3. Study of lipid composition in biological membranes of MDCK II - hBest1 cells**

Changes in TER of MDCK II - hBest1 cells raised the question of lipid composition and structures (heterogeneity) in their biological membranes. The structure and functions of any transmembrane protein, such as hBest1, depend on the lipid environment. In transfected MDCK II cells, we found differences in several key lipid fractions compared to untransfected cells. In MDCK II - hBest1 cells, higher amounts of phosphatidylinositol and phosphatidate (PI+PA, 90% more) were detected in the mixed fraction, cardiolipin (DPG, 75% more), as well as for the lysolipids lysophosphatidylcholine, lysophosphatidylethanolamine (LPC, 42% more and LPE, 33% more) and the indeterminate fraction A (fr A, 25% more). In non transfected cells, higher amounts of neutral lipids (NL – 20% more), phosphatidylserine (PS, 33% more), phosphatidylcholine (PC, 13% more) as well as the unknown fraction C ( fr C, 53% more) were observed (**Figure 15**).

These data support the TER studies (**Figures 11, 12, 13, 14**) in which MDCK II - hBest1 cells are more resistant to the enzymatic action of sPLA<sub>2</sub>, which may be due to the reduced amount of PC and the increased amount of lysolipids against which the enzyme has no or has low activity. A similar difference in phospholipid composition exists in MDCK II cells (about 58% PC and 28% PE) and RPE cells (in which hBest1 is endogenously expressed, about 20% PC and 67% PE). These data confirm that the **expression of hBest1 in cells is associated with the increased accumulation and/or biosynthesis of non lamellar lipids in membranes** compared to lamellar lipids. There is also a connection between the change in lipid biosynthesis (metabolism) and the development of some pathology, for example, with the accumulation of cholesterol in the RPE during the development of Best disease. An increase in cholesterol can lead to membrane remodeling and a change in the functions of membrane proteins. This points to the possible role of mutant forms of hBest1 in membrane remodeling by altering the quantitative balance between lamellar/non lamellar lipids and the (non)formation of lipid rafts in the initiation and development of various pathological conditions.

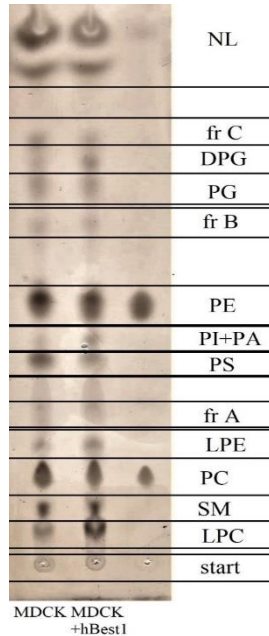


**Figure 15.** Thin layer chromatography of lipid extracts from MDCKII and MDCKII-hBest1 cells. Legend: NL – neutral lipids; fr C – unknown fraction C; DPG – cardiolipin; PG – phosphatidylglycerol; fr B – unknown fraction B; PE – phosphatidylethanolamine; PI – phosphatidylinositol; PA – phosphatidic acid; PS – phosphatidylserine; fr A - unknown fraction A; LPE – lysophosphatidylethanolamine; PC – phosphatidylcholine; SM – sphingomyelin; LPC – lysophosphatidylcholine.

#### 1.2.4. Association of hBest1 with lipid rafts in biological membranes of MDCK II - hBest1 cells

By Laurdan staining, the difference in membrane heterogeneity was demonstrated in untransfected MDCK II and MDCK II - hBest1 alive cells. An increase in  $L_d$  domains was observed in the membranes of hBest1 transfected cells compared with the  $L_d$  domains of untransfected cells. GP (Generalised Polarization) images and GP values derived from histograms indicate **a lower degree of molecular ordering or greater “fluidity” in the cell membranes of MDCK II - hBest1 cells**. This is because lower order correlates with lower GP values (0.472) and increased green signal in membranes of transfected cell compared to higher GP values (0.575) and increased yellow-red signal in membranes of untransfected MDCK II cells (**Figure 16**). This effect of hBest1 confirms the results obtained for the lipid composition in the membranes of MDCK II - hBest1 cells, in which a greater amount of non lamellar lipids is observed, leading to membrane fluidization and an increase in  $L_d$  domains in them.

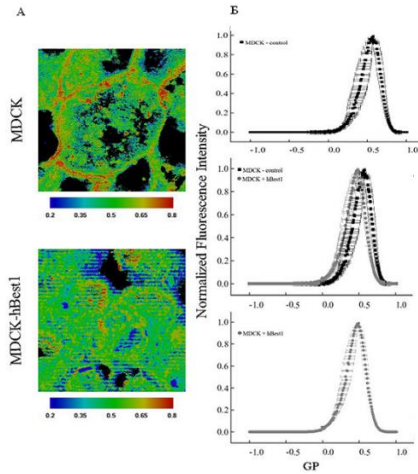


**Figure 16.** A) GP images and B) histograms represent low ordered (green color - lower GP values) and high ordered membrane domains (yellow-red color - higher GP values) in alive MDCK II and MDCK-hBest1 cells. Data are represented as mean  $\pm$  SE,  $n = 30$ ,  $p < 0.01$ . The p-value has been estimated only for the GP peak maximums of MDCK II and MDCK-hBest1 cells. (Mladenov et al., 2020).

Immunofluorescence of hBest1 visualized its **predominant localization in the less ordered  $L_d$  regions** of the cell membrane (65%), versus 35% in the more ordered  $L_o$  domains (lipid rafts) (Figure 17).

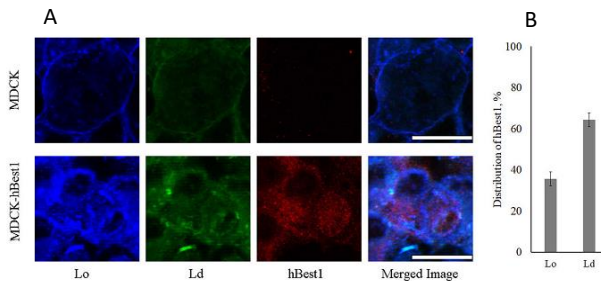


**Figure 17.** A) Fluorescent signals of hBest1 (red) and Laurdan stained  $L_o$  (blue) and  $L_d$  (green) regions of membranes in alive MDCK II and MDCK-hBest1 cells. B) Distribution of the amount of hBest1 in  $L_o$  and  $L_d$  regions of alive MDCK-hBest1 cell membranes. Data are represented as mean  $\pm$  SE,  $n = 6$ ,  $p < 0.001$ . The white scale bar = 10  $\mu$ m. (Mladenov et al., 2020).

A similar heterogeneity of association was also observed in the distribution of hBest1 in DRM ( $L_o$  - like microdomains) and DSM ( $L_d$  - like microdomains) isolated from MDCK II - hBest1 cell membranes (after solubilization with the nonionic

detergent Triton X-100). The data obtained show about 30% localization of hBest1 in the DRM and 70% in the DSM despite the physicochemical characteristics of the detergent-membrane interactions and limitations in the experimental setup.

The partial distribution of hBest1 between  $L_o$  and  $L_d$  phases depends on the lipid and protein composition, structure, physicochemical and biochemical characteristics of biological membranes. This distribution has a direct effect on the structure, oligomerization and function of hBest1. Due to the association of about 70% of hBest1 to  $L_d$  and DSM, the probability that lipid rafts have a negative rather than a positive effect on protein activation is greater, which is indirectly confirmed by the experiments performed with the effect of sPLA<sub>2</sub> on the increase in TER (see above).

### **1.3. Effect of hBest1 mutant forms Y85H, Q96R, R25W and Y227N in stabilizing their expression on MDCKII cells**

Mutant forms of hBest1 - Y85H, Q96R, R25W and Y227N, which cause BVMD, show impaired BI localization when transiently expressed in MDCKII cells (see above). Stabilization of the expression of these mutants in RPE-1 and MDCKII cells, as with normal hBest1, was not achieved because the cells died two weeks after incubation in selective medium (containing G418). For this reason, our study focused on analyzing the survival of MDCKII cells transfected with these mutant forms of the protein by examining apoptosis. The measurement of the apoptosis levels of the transfected cells was performed during subculturing of the cells in the selective medium (first measurement) and on the third day after incubation of the cells in the selective medium (second measurement).

In both measurements, cells transfected with wild-type protein showed the highest survival (about 75% and 40%). In cells transfected with the mutant forms, at the first measurement, we reported an **increase** in early (up to 28%) and late (up to 38%) apoptosis. In the second measurement of cells transfected with mutant forms, unaffected cells were below 30%. Here again, a higher levels of early (over 50%) and late (about 15-20%) apoptosis was observed. One of the highest levels of apoptosis was found in cells transfected with Y227N mutants, and their toxic effect was observed immediately after transfection. The toxicity of these mutant forms, which occurs on the third day of selection, severely limits the preparation and isolation of stable cell lines. In addition to the increased Ap localisation of the different mutant forms of hBest1, the change in ion transport and cellular homeostasis, their toxic action may also be related to the change in lipid balance and phase state, which would cause membrane dysfunction (Ap and BI have a specific lipid profiles). Therefore, other, alternative approaches for transfection, selection and stabilisation of cells transfected with hBest1 mutants are needed.

### **1.4. Summary of results obtained from hBest1 cell culture studies**

These studies started with the selection of an appropriate cell line and the potential basolateral sorting motifs in the hBest1 molecule. Our results indicated that:

- Retinal cells from the RPE-1 and RPE-J lines are not suitable for studying hBest1 sorting, due to overlapping of cells during monolayer formation in the process of cell polarization.

- Epithelial cells of the MDCK II line are a good model to study hBest1 sorting, due to the formation of a typical monolayer with well defined apical and basolateral membranes in the process of cell polarization.

- Upon transient transfection of normal hBest1, the protein localized to the basolateral membrane in polar MDCK II cells, similar to cells in the RPE, ie. both cell lines similarly interpret the sorting signals in the hBest1 molecule.

- **Disturbances in the composition and structure of the potential basolateral sorting motifs Y85VTL, Y97ENL and Y227DWI cause an increase in the apical localization of hBest1 mutant forms (15% for p.Y85H ( $P = 5.37 \times 10^{-5}$ ), 10% for p.Q96R ( $P = 0.0001$ ), 6% for p.L100R ( $P = 0.0009$ ) and 9% for p.Y227N ( $P = 5.20 \times 10^{-5}$ ).**

- A complete “reversal” in the localization of mutant proteins with disrupted sorting motifs is lacking, so it is possible that several motifs are involved in sorting and have a cumulative effect on hBest1 localization. Furthermore, tyrosine phosphorylation is most likely part of the sorting process.

Research continues with the establishment and characterization of stable cell lines expressing hBest1.

- The stable RPE-1 - hBest1 cell line expressing wild type hBest1 was established, but the resulting hBest1 translation signal was very weak. Cells of the line showed reduced values in growth rates, mitotic index and metabolic activity, altered morphology (increased cell volume) and increased TER compared to non transfected cells. For these reasons, this line was not used in further studies.

- **The new stable MDCK II - hBest1 cell line expressing wild-type hBest1 was established in which the resulting hBest1 translational signal was sufficiently strong. Growth characteristics, metabolic activity, and cell morphology remained unchanged as in untransfected cells. For these reasons, this line was used in the following studies.** Stabilizing the expression of the hBest1 mutant forms Y85H, Q96R, R25W and Y227N always induces apoptosis and death of MDCK II cells, so it has not been possible (so far) to generate stable cell lines expressing them. The creation of the new MDCK II - hBest1 line, was the first critical step in hBest1 studies, which predetermined the research that followed.

- hBest1 localizes to the basolateral membrane in six-day-old polarized MDCK II - hBest1 cells (does not change cell polarization time).

- TER in the process of polarization of MDCK II - hBest1 cells (between the fourth and seventh day) showed lower transmembrane resistance values (115 - 125  $\Omega$ ) compared to MDCK II cells (133 - 140  $\Omega$ ). Maximum TER values were reached between days eight and nine in transfected (140–150  $\Omega$ ) compared to non-transfected (140  $\Omega$ ) MDCK II cells (days five and six). The delay in reaching maximum TER values in MDCK II - hBest1 cells showed that cell polarization is not always associated with the synchronous increase in transepithelial resistance.

- The high TER values we obtained with the addition of Glu and GABA and the low values with the addition of ATP suggest a decrease and an increase in hBest1 activity, respectively.

- We found a strong effect of sPLA<sub>2</sub> on untransfected cells and a decrease in TER (about 20%) in contrast to the TER of the monolayer of MDCK II - hBest1 cells, where minimal changes were observed (below 10%). Transfected cells were more resistant to the enzymatic action of sPLA<sub>2</sub>.

- We found that the expression of hBest1 in cells is associated with the increased accumulation and/or biosynthesis of non lamellar lipids in membranes compared to lamellar lipids, which determines the stronger resistance to sPLA<sub>2</sub>.

- An increase in L<sub>d</sub> domains was observed in the membranes of hBest1 transfected cells compared to L<sub>d</sub> domains in untransfected cells.

- We found that hBest1 localizes and self-organizes in the less ordered L<sub>d</sub> domains of the cell membrane (about 60–65%), compared to 30–35% in the more ordered L<sub>o</sub> domains (lipid rafts).

How hBest1 interacts with individual lipids in the L<sub>o</sub> and L<sub>d</sub> domains of biological membranes, how its conformation, molecular organization, and activity changes have been the subject of further discussion and additional studies with models of biological membrane.

## 2. Studies of hBest1 in models of biological membranes

### 2.1. Isolation and purification of hBest1 from MDCK II - hBest1 cells

For the isolation of hBest1, cells from the newly established line MDCK II - hBest1 were used.

Optimization of the hBest1 purification protocol involved different combinations and sequences of purification methods (mainly gel filtration and affinity chromatography) and buffer variants.

Best results were obtained by applying gel filtration chromatography as a first step immediately after cell lysis. After lysis and each purification step, samples containing hBest1 were dialyzed against the appropriate elution buffer. The elution profile from the Superose 12 column was followed by measuring the absorbance at 280 nm (**Figure 18**). Thus, the samples were purified from the multicomponent lysis buffer and the low and high molecular weight cellular proteins were removed (**Figure 19A**). hBest1 signal with an expected size of 68 kDa was detected in fractions no. 34 and 35, which was also demonstrated by Western blot analysis (**Figure 18**). Affinity chromatography was used as a second step in the purification - we applied the combined fractions containing His-linked hBest1 to a HisTrap column. All fractions collected at this stage were reanalyzed by Western blot and hBest1 was visualized as a single band of 68 kDa (**Figure 19B**). By Smith's method, the yield of pure His-linked hBest1 isolated from MDCK II cells was found to be about 2.8% (based on total protein content in total cell lysates).

Using this optimized two-step purification scheme ensured that a large amount of purified hBest1 was obtained to be used in future studies.

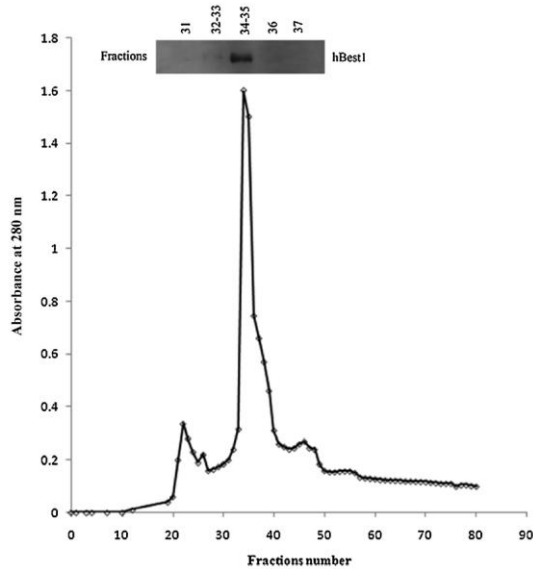


**Figure 18.** Purification of hBest1 from hBest1 stably transfected MDCK cell line - Superose 12 column HR 10/30 gel-filtration chromatography and Immunoblotting of fractions enriched with hBest1 protein. (Mladenova et al., 2014).

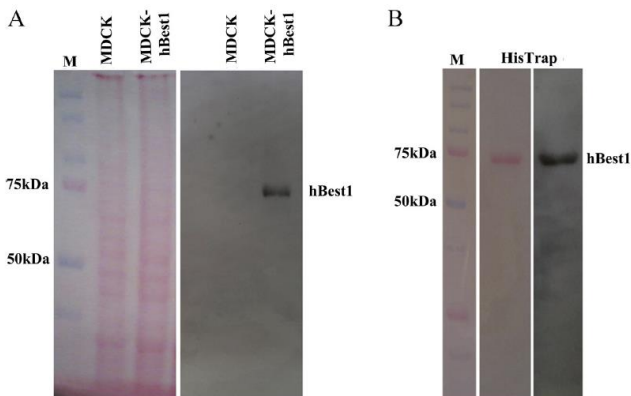


**Figure 19.** Ponceau S staining (red) and immunodetection of hBest1: (A) total lysates: MDCK II; MDCK II - hBest1; M (protein markers); (B) purified hBest1 protein after affinity chromatography step on HisTrap. hBest1 protein is detectable as a 68 kDa band. (Mladenova et al. 2014).

## 2.2 Analysis of secondary structure elements of the hBest1 protein by FTIR spectroscopy

The secondary structure of human Best1 **has not yet been described**, so our studies with models of biological membranes started with the determination of secondary structural elements (in the absence and presence of  $\text{Ca}^{2+}$ ) by FTIR spectroscopy. **Figure 20A** shows the amide I and amide II regions in the FTIR spectra of aqueous solutions of hBest1 and hBest1<sup>Ca</sup>.

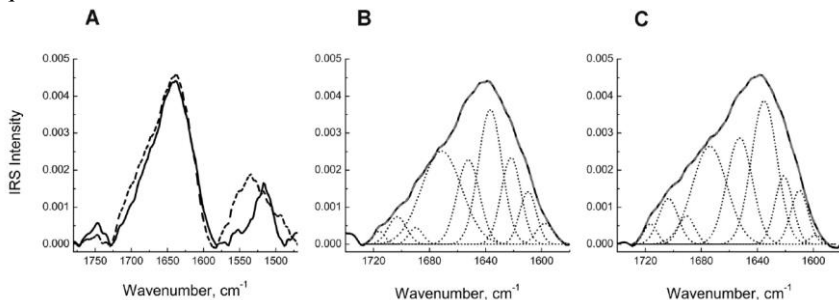


**Figure 20.** (A) FTIR spectra of hBest1 (black curve) and hBest1<sup>Ca</sup> (discontinuous curve) in the amide I (centered at 1638  $\text{cm}^{-1}$ ) and II (assigned at 1534  $\text{cm}^{-1}$  for hBest1 and 1517  $\text{cm}^{-1}$  for hBest1<sup>Ca</sup>) regions. Decomposition components (dotted lines) and Gaussian fits (discontinuous gray lines) with correlation factor  $R \geq 0.9998$ , completely matching the original IRS - spectra (black lines) of (B) hBest1 and (C) hBest1<sup>Ca</sup> (Mladenova et al., 2017).

Sample	WN, $\text{cm}^{-1}$	Assignment	Relative content, %	
hBest1	1716	COOH group of sidechain-aspartic and glutamic acids (protonated form)		
	1703	COOH group of sidechain-aspartic and glutamic acids (with two hydrogen bonds)		
	1690	anti-parallel $\beta$ -sheets	2.0	
	1671	$\beta$ -turns and loops	32.2	
	1652	$\alpha$ -helix	16.3	
	1637	$3_{10}$ -helix	27.2	
	1622	aggregated $\beta$ -sheets	14.7	
	1610	short helices	7.6	
	hBest1 <sup>Ca</sup>	1716	COOH group of sidechain-aspartic and glutamic acids (protonated form)	
		1703	COOH group of sidechain-aspartic and glutamic acids (with two hydrogen bonds)	
1690		anti-parallel $\beta$ -sheets	3.7	
1674		$\beta$ -turns and loops	27.2	
1653		$\alpha$ -helix	21.9	
1635		$3_{10}$ -helix	29.8	
1621		aggregated $\beta$ -sheets	9.9	
1610		short helices	7.5	
	1598	Sidechain-tyrosine in deprotonated state		

**Table 1.** Amide I decomposition components of hBest1 and hBest1<sup>Ca</sup> FTIR-spectra: wavenumber position, peak assignment, and relative content in %. (Mladenova et al., 2017).

We found that the secondary structure composition of hBest1 (**Figure 20B and Table 1**) includes predominantly **helical structural elements (51.1%), including large and short  $\alpha$ -helices (total 23.9%) and  $3_{10}$  - helices (27.2 %)**. Addition of  $\text{Ca}^{2+}$  induced conformational changes by increasing all helical structures to 59.2%, mainly due to an increase in  $\alpha$ -helix content (by 5.6%), while the increase in  $3_{10}$ -helices and short helical regions remained small (**Figure 20C and Table 1**).

FTIR spectra indicated that the protein secondary structure was considerably altered under the treatment with  $\text{Ca}^{2+}$ , manifested by **increase of the helical structures** in favor of the short connecting chains. Binding of  $\text{Ca}^{2+}$  causes and stabilizes certain conformational changes in the structure of hBest1, most likely determining the functional activity of the protein molecules.

### 2.3. Investigation of the surface properties of hBest1 in Langmuir monolayers and Langmuir-Blodgett films

#### 2.3.1. Effects of $\text{Ca}^{2+}$ , Glu and GABA on the $\pi/A$ isotherms and hystereses of Langmuir monolayers of hBest1

In addition to  $\text{Ca}^{2+}$  induced changes in hBest1 structure, the transport of neurotransmitters (such as Glu, GABA, serotonin, etc.) across cell plasma membranes can also induce various conformational changes in protein transporters and the membranes themselves. These changes make a physicochemical understanding of the influence of  $\text{Ca}^{2+}$ , Glu, and GABA on the structural and surface properties of hBest1 key to elucidating its functions. We therefore performed the studies to determine the effects of  $\text{Ca}^{2+}$ , Glu, and GABA on the surface activity and behavior of hBest1 in Langmuir monolayers under physiological conditions. Surface pressure/area ( $\pi/A$ ) isotherms allow the detection of even very small changes in molecules such as size, conformation or the presence of double bonds that can alter the lateral organization of the monolayer. The  $\pi/A$  isotherms of monolayers of hBest1, hBest1 $^{\text{Ca}}$ , hBest1Glu and hBest1GABA are compared in **Figure 21**.

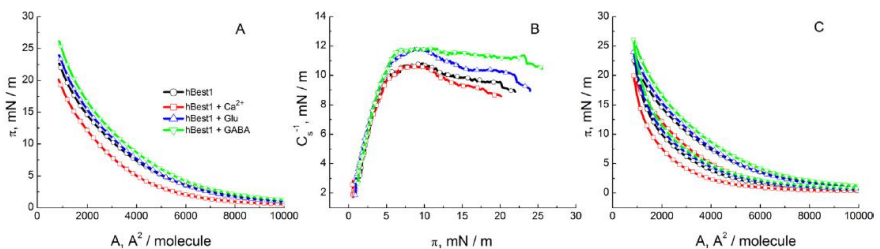


**Figure 21.** A) Surface pressure/mean molecular area ( $\pi/A$ ) isotherms; B) compressibility moduli,  $C_s^{-1}$ , versus surface pressure ( $\pi$ ) and C)  $\pi/A$  hysteresis loops of hBest1 monolayers at the air/water interface. The subphases contain 150 mM NaCl with addition of  $\text{Ca}^{2+}$ , Glu and GABA (Andreeva et al., 2018).

The curves of all isotherms have the same smooth shape and are almost parallel to each other. The decrease in mean molecular area during compression leads to an increase in surface pressure, but without the formation of plateaus or kinks in the isotherms that indicate the presence of conformational and phase transitions. The initial values of the surface pressure during the spreading of the hBest1 monolayers ( $\pi_0 = 0.7$  mN/m) change when the different components are added – with  $\text{Ca}^{2+}$  it decreases and is

the lowest ( $\pi_0 = 0.4$  mN/m), and with GABA increases and is highest ( $\pi_0 = 1.2$  mN/m). As a result, the compression isotherms of hBest1Ca and hBest1GABA monolayers are shifted to lower and higher surface pressures at a given molecular area and lower and higher surface area per molecule at a given pressure, respectively, compared to the isotherms of pure hBest1. The  $\pi/A$  isotherms show that the addition of  $\text{Ca}^{2+}$ , Glu, and GABA induces changes of the mean molecular area ( $A$ ) of hBest1 as follows:  $A^{\text{Ca}^{2+}} < A^{\text{NaCl}} \leq A^{\text{Glu}} < A^{\text{GABA}}$ . By extrapolating the slope of the steep part of the isotherms, at high two-dimensional pressures, to zero pressure, we determined the lowest (smallest) possible area per molecule,  $A_0$ , to which the monolayer can be compressed without collapse, which for hBest1<sup>Glu</sup> and hBest1<sup>GABA</sup> is similar to that of the hBest1 monolayer ( $A_0 = 3700 \text{ \AA}^2/\text{monomer}$ ) and significantly lower for hBest1<sup>Ca</sup> ( $A_0 = 3360 \text{ \AA}^2/\text{monomer}$ ). Crystallographic analysis of the Best1-Fab complexes yielded dimensions of  $70 \times 70 \text{ \AA}$  for one monomer, giving an area of approximately  $3850 \text{ \AA}^2/\text{monomer}$ . The values of the limiting areas for hBest1, hBest1<sup>Glu</sup> and hBest1<sup>GABA</sup> are close to those of chBest1, while the reduction of  $A_0$  in the presence of  $\text{Ca}^{2+}$  is probably the result of the complex interplay between several factors, including the change of molecular electrostatic interactions, the difference in molecular packing density, the conformation and the orientation of hBest1 molecules on the film surface. In monolayers with and without Glu and GABA, the  $A_0$  limiting areas are similar, while the regions at a given two-dimensional pressure differ, again indicating a different organization and packing density of the protein molecules. Addition of  $\text{Ca}^{2+}$ , Glu, and GABA to a monolayer of hBest1 changes the monomer area per molecule  $A_{20}$  (at 20 mN/m) in the order:  $A_{20}^{\text{Ca}^{2+}}$  ( $840 \text{ \AA}^2/\text{molecule}$ )  $<$   $A_{20}^{\text{NaCl}}$  ( $1130 \text{ \AA}^2/\text{molecule}$ )  $<$   $A_{20}^{\text{Glu}}$  ( $1300 \text{ \AA}^2/\text{molecule}$ )  $<$   $A_{20}^{\text{GABA}}$  ( $1490 \text{ \AA}^2/\text{molecule}$ ). In all cases, these areas are lower than the crystallographic area, possibly due to extrusion of the protein molecules to the aqueous phase during compression. Similar behavior has been observed in monolayers of other proteins, where increasing the salt concentration decreases the "sinking" of the molecules, allowing the determination of the actual/real monomer area.

Changes in elasticity and structure of hBest1 monolayers were analyzed by compressibility moduli versus surface pressure ( $C_s^{-1}/\pi$ ) curves (**Figure 21B**). We found that two regions can be distinguished: a first with a relatively steep growth of  $C_s^{-1}$  during the initial compression up to  $\sim 7$  mN/m, due to the reorganization and compaction of the molecules, and a second after reaching a maximum – a slow gradual decrease in compressibility moduli until the end of compression, suggesting a reorientation of the protein molecules at the surface and less stability of the monolayers at  $\pi > 11$  mN/m. The maximum compressibility moduli ( $C_s^{-1}(\text{max}) = 10.7$  mN/m for hBest1 and hBest1<sup>Ca</sup> and  $C_s^{-1}(\text{max}) = 11.8$  mN/m for hBest1<sup>Glu</sup> and hBest1<sup>GABA</sup>) are at the lower limit of this characteristic for liquid-extended (LE) lipid films (ranging from 12.5 to 50 mN/m).

Additional information about the molecular interactions, structural rearrangements and stability in the monolayers is provided by the compression-decompression hysteresis of the  $\pi/A$  isotherms. We therefore compared the  $\pi/A$  hysteresis loops of hBest1 films (**Figure 21C**). We found that the decompression curves shifted to lower molecular areas, suggesting that the films are in different states during

compression and decompression. The difference in area between the compression and expansion branches, at any fixed surface pressure, i.e. hysteresis,  $\Delta A^\pi$ , increases in the following order:  $\Delta A^{\text{Ca}^{2+}} < \Delta A^{\text{NaCl}} \leq \Delta A^{\text{Glu}} < \Delta A^{\text{GABA}}$ . Data show that all monolayers studied have significant hysteresis, which decreases with increasing  $\pi$ . Only for hBest1<sup>Ca</sup> monolayers do the horizontal  $\pi/A$  branches of compression and decompression coincide, indicating that the final state of the monolayer is the same at the end of expansion and at the beginning of compression, i.e. both processes are completely reversible. We assume that in the presence of  $\text{Ca}^{2+}$ , the more hydrophobic hBest1 protein molecules that are pushed into the subphase at increased surface pressure, returned back during decompression. Even measurements of two consecutive compression/decompression cycles show that they completely coincide, confirming that the “sinking” of the molecules of the hBest1<sup>Ca</sup> film in the subphase is a reversible process. For hBest1, hBest1<sup>Glu</sup> and hBest1<sup>GABA</sup> monolayers, the surface pressure values at the end of expansion were 0.5 mN/m lower than at the beginning of compression, suggesting either irreversible changes in the organization and/or orientation of the protein molecules, or “non-return” protein aggregates formed during compression to their original state after decompression. When repeating the compression–decompression of the monolayer, the cycle starts and ends at the same  $\pi$  at which the first one ends. Both cycles coincide at  $\pi > 15$  mN/m, suggesting that the submerging of hBest1 in the subphase is a reversible process and is not the reason for the discrepancy between the initial and final values of the surface pressure, but is most likely due to reorientation and reorganization of the protein molecules on the surface of the monolayer.

### **2.3.2. Effects of $\text{Ca}^{2+}$ , Glu and GABA on the morphology of Langmuir monolayers of hBest1**

The next step in the study of Langmuir monolayers of hBest1 in the presence of  $\text{Ca}^{2+}$ , Glu, or GABA was to visualize the surface of the films by Brewster angle microscopy (at a given  $\pi$  corresponding to the  $\pi/A$  isotherms) and determine their morphology. BAM images were taken of hBest1 monolayers in the presence and absence of  $\text{Ca}^{2+}$ , Glu, and GABA, 30 min after monolayer construction before compression (**Figure 22, 1<sup>st</sup> column**) and at a surface pressure of 20 mN/m (**Figure 22, 2<sup>nd</sup> column**).

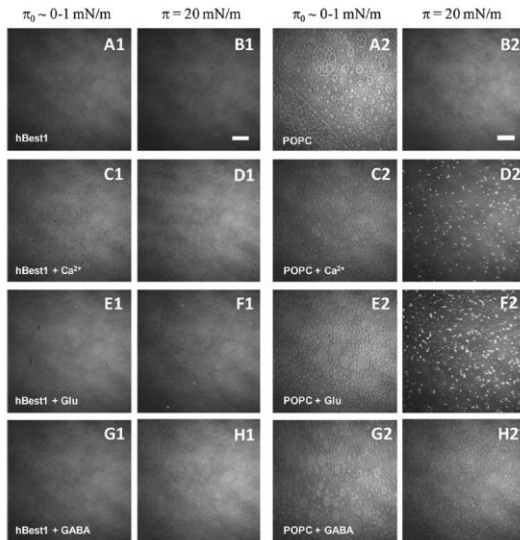


**Figure 22.** BAM images of hBest1 (columns 1 and 2) and POPC (columns 3 and 4) films on water substrates containing 150 mM NaCl (A1, B1, A2, B2) with addition of  $0.5\mu\text{M}\text{Ca}^{2+}$  (C1, D1, C2, D2), 2 mM Glu (E1, F1, E2, F2) and 100  $\mu\text{M}$  GABA (G1, H1, G2, H2), taken 30 min post spreading of uncompressed monolayers and at 20 mN/m. The whitebars represent 100  $\mu\text{m}$ . (Andreeva et al., 2018).

Based on the BAM images and  $\pi/A$  isotherms, we can claim that the monolayers of hBest1, hBest1<sup>Ca</sup>, hBest1<sup>Glu</sup>, and hBest1<sup>GABA</sup> have different packing densities as a result of the change in protein conformation, protein-protein interactions, and the change in protein macro- and self-organization at the air/buffer interface. However, BAM did not allow distinguishing the exact conformations of hBest1 protein complexes before and after treatment with  $\text{Ca}^{2+}$ , Glu or GABA, so our studies continued with the use of AFM, which enabled the visualization of nanoscale changes, structure and organization of protein molecules .

### 2.3.3. Effects of $\text{Ca}^{2+}$ , Glu and GABA on the topology of hBest1 Langmuir-Blodgett films

In the studies described so far, we have shown that hBest1 possesses significant surface activity and forms stable Langmuir monolayers at the air/buffer interface, which allowed us to perform the so-called Langmuir-Blodgett transfer of compact hBest1 films from aqueous (150 mM NaCl, pH 7) to solid support and subsequent visualization by AFM. We found that hBest1 molecules have an oval shape with lateral dimensions (after deconvolution) of  $100 \times 160 \text{ \AA}$  and a height of  $75 \text{ \AA}$  (**Figure 23A**) (all data are shown in **Table 2**), and these dimensions of the protein exceed the values of  $70 \times 70 \text{ \AA}$  and height  $95 \text{ \AA}$ , which were calculated for chBest1.

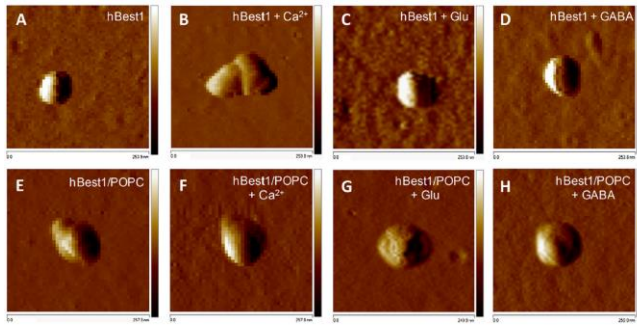


**Figure 23.** Typical error-mode AFM images of hBest1 molecule. The scanned area is about  $250 \times 250$  nm. (Andreeva et al., 2018).

Sample	Lateral dimensions, Å	Height, Å
<b>hBest1</b>	$100 \times 160 (\pm 20)$	$75 (\pm 10)$
+Ca <sup>2+</sup>	$200 \times 670 (\pm 20)$	$220 (\pm 20)$
+Glu	$180 \times 220 (\pm 20)$	$80 (\pm 10)$
+GABA	$180 \times 220 (\pm 20)$	$100 (\pm 10)$
<b>hBest1/POPC</b>	$230 \times 260 (\pm 20)$	$120 (\pm 10)$
+Ca <sup>2+</sup>	$280 \times 330 (\pm 20)$	$120 (\pm 10)$
+Glu	$220 \times 240 (\pm 20)$	$100 (\pm 10)$
+GABA	$260 \times 310 (\pm 20)$	$150 (\pm 15)$

**Table 2.** hBest1 lateral dimensions and height, obtained from the AFM images, after tipsample deconvolution ( $\pm$ standard deviation) (Andreeva et al., 2018).

This discrepancy may be due to both the larger AK sequence of hBest1 (585 AK for hBest1) and the specificity of the methods used. Addition of Ca<sup>2+</sup> changes the secondary structure of hBest1, causing a powerful effect in which protein aggregation (dimerization and trimerization) is induced (Figure 23B and Tables 1 and 2). The increased sizes of hBest1 in the presence of Ca<sup>2+</sup> indicate the existence of a completely new ordered oligomeric structure due to the induced conformational changes and not just the simple sum of the individual molecules. Ca<sup>2+</sup> induced formation of oligomeric (higher order) structures has been demonstrated for hBest1 homologues and a number of other proteins. The presence of Ca<sup>2+</sup> leads to the formation of stable pentameric crystals, which have been reported for KpBest and chBest1 in complex with monoclonal antibody Fab-fragments. However, the oligomerization of hBest1 (formation of dimeric, tetrameric, or pentameric structures) is still under discussion. In contrast, no aggregation of molecules was observed after treatment with Glu and GABA. hBest1 retained its original oval shape and height, but increased its lateral dimensions to some extent ( $180 \times 200$  Å) as a result of reorientation and/or alteration of its structure (Figure 23C, D and Table 1).

## 2.4. Effects of $\text{Ca}^{2+}$ , Glu and GABA on the $\pi/A$ isotherms and hystereses of hBest1/POPC Langmuir monolayers

Studies of the surface properties of hBest1 continued with the construction of near natural models of biological membranes, such as composite Langmuir monolayers (the multicomponent monolayers containing proteins and lipids). To study the properties of binary hBest1/POPC monolayers, we used such model membranes in which the ratio of the area occupied by protein to that occupied by surrounding lipids is 1:3. At a surface pressure of 20 mN/m, the surface area of one hBest1 molecule ( $1150 \pm 20 \text{ \AA}^2$ ) (**Figure 21A**) is 15 times higher than that of one POPC molecule ( $78 \pm 2 \text{ \AA}^2$ ) (**Figure 24A**), which determines the molar ratio of the two components for the binary hBest1/POPC Langmuir monolayers to be 1/45. The  $\pi/A$  isotherms of bicomponent hBest1/POPC (1:45) monolayers, in the presence and absence of  $\text{Ca}^{2+}$ , Glu, and GABA in the aqueous subphase, are shown in **Figure 24A**.

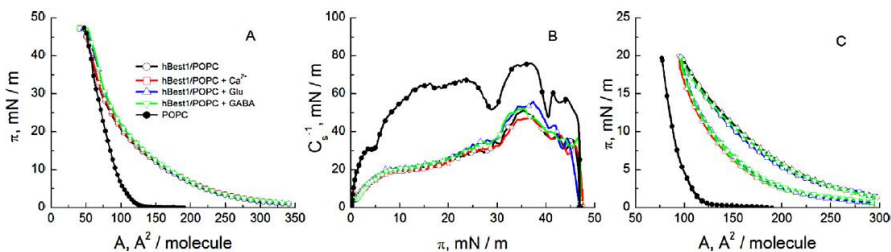


**Figure 24.** **A)** Surface pressure/mean molecular area ( $\pi/A$ ) isotherms; **B)** compressibility moduli  $C_s^{-1}$ , versus surface pressure ( $\pi$ ); **C)**  $\pi/A$  hysteresis loops of mono-component POPC (they match and are represented as colorless squares and black-filled circles) and two-component hBest1/POPC (1/45) monolayers at the air/water interface containing 150 mM NaCl with addition of  $\text{Ca}^{2+}$ , Glu and GABA (Andreeva et al., 2018).

For comparison, the isotherm of POPC film is also presented in the figure and shows that the monolayer was in the LE phase until its collapse at 46 mN/m. The  $\pi/A$  isotherms of POPC as well as the isotherms of hBest1/POPC monolayers in the presence and absence of  $\text{Ca}^{2+}$ , Glu, and GABA are indistinguishable from each other and have an identical course. The second-order phase transition between two condensed states of the monolayer is known to exhibit a kink of the  $\pi/A$  isotherms. Since none of the components of the composite films form condensed phases, the kink observed at  $\sim 31$  mN/m ( $\pi_{tr}$ ) (this is the packing pressure found in biological cell membranes) in the  $\pi/A$  isotherms of hBest1/POPC films shows the collapse of one of the components. At surface pressures below  $\pi_{tr}$ , the  $\pi/A$  isotherms of hBest1/POPC films closely resembled those of hBest1 monolayers (**Figure 21A**), despite its mole fraction being only 1/45. At  $\pi > \pi_{tr}$  (above 35 mN/m), the isotherms become steeper and overlap with those of POPC.

According to the Gibbs phase rule applied to Langmuir films, the number of degrees of freedom  $F$  of a two-component monolayer at constant temperature and atmospheric pressure is  $F = 2 - q$ . If the components are immiscible and form two surface

phases ( $q = 2$ ), the system has no degrees of freedom  $F = 0$  and the collapse surface pressure,  $\pi_{\text{col}}$ , (at which the material appears in the 3D bulk phase) is independent of the monolayer composition. Accordingly, the changes of  $\pi_{\text{col}}$  depending on the composition of the film are an indication of molecular mixing of the components. It can be seen from **Figure 24A** that the  $\pi_{\text{col}}$  of the hBest1/POPC monolayers overlaps with that of the POPC monolayer (46 mN/m), therefore hBest1 and POPC are immiscible at the air/buffer interface. These results suggest that the compression of the binary monolayers leads to the extrusion of the protein molecules to the aqueous phase and for  $\pi > \pi_{\text{tr}}$  the surface mainly contains the lipid molecules, which at compression up to 46 mN/m pass into the bulk phase and the film collapse. Therefore, the kink in the  $\pi/A$  isotherms of the monolayers represents the end of protein extrusion into the aqueous subphase.

The  $C_s^{-1}/\pi$  dependences of POPC and hBest1/POPC monolayers showed a similar trend (**Figure 24B**). No plateaus and/or any vertical “jumps” in the compressibility moduli were observed, but they gradually increased to  $\sim 31$  mN/m ( $\pi_{\text{tr}}$ ) and then became steeper, reaching a maximum of  $\sim 45$  mN/m, where are the inflection points of the  $\pi/A$  isotherms. The sharp decrease in  $C_s^{-1}$  at  $\sim 46$  mN/m indicates that the films undergo collapse. The compressibility moduli of the four composite films at each surface pressure are very similar, confirming that they are in the same phase state. The maximum compressibility moduli of the POPC monolayers were 1.5 times higher than those of the hBest1/POPC monolayers, indicating the **“fluidization” effect of the protein molecules on the POPC films and the increased elasticity of the composite monolayers**.

In subsequent studies, to avoid the extrusion of protein molecules into the subphase, we determined the hysteresis of two component monolayers by compression to 20 mN/m (below  $\pi_{\text{tr}}$ ) followed by immediate expansion. We found no statistically significant effect of  $\text{Ca}^{2+}$ , Glu, and GABA on the hysteresis of the composite monolayers (**Figure 24C**). The compression and decompression curves of the POPC monolayer match perfectly, therefore the significant hysteresis of the composite monolayers can only be attributed to the hBest1 molecules. The shape of the hysteresis branches of hBest1/POPC films resembled those of hBest1 (**Figure 21C**). Also, the decompression curves were located at lower molecular areas (for any  $\pi$ ) and lower surface pressures (for any  $A$ ). The significantly lower surface pressure values at the end of expansion suggest an irreversible reorganization and/or reorientation of protein molecules in the monolayer during compression, regardless of the presence or absence of  $\text{Ca}^{2+}$ , Glu, or GABA. Therefore, POPC eliminated the effects of  $\text{Ca}^{2+}$ , Glu and GABA on pure hBest1 monolayers (**Figures 21C and 24C**).

We continued with an analysis of the behavior of binary monolayers at the air/liquid interface, and to demonstrate the miscibility and ideal/non-ideal character of binary monolayers, we compared the average molecular areas  $A_\pi$  (measured at surface pressures of 10 and 20 mN/m, below  $\pi_{\text{tr}}$ ) with the corresponding molecular areas  $A_{\text{add}}$  for an ideal mixture or complete phase separation, which in both cases follows the additivity rule (**Figure 25A**):  $A_{\text{add}} = X_{\text{hBest1}}A_{\text{hBest1}} + X_{\text{POPC}}A_{\text{POPC}}$

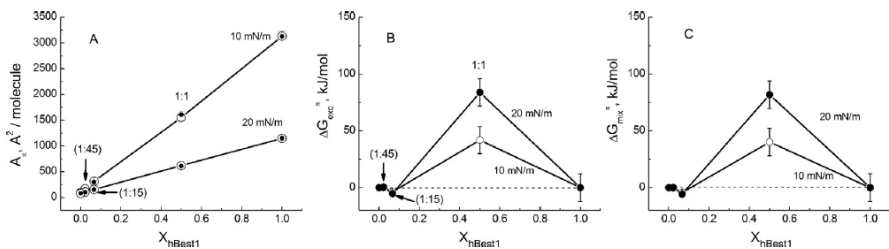


**Figure 25.** **A)** Experimental molecular area of the mixtures (●) and the corresponding molecular area  $A_{\text{add}}$  for ideal mixture (○) (the error bars are within the limits of the symbols); **B)** Excess free energy of mixing  $\Delta G_{\text{exc}}^{\pi}$  and **C)** total free energy of mixing  $\Delta G_{\text{mix}}^{\pi}$  in the binary hBest1/POPC monolayers at 10 and 20 mN/m as a function of  $X_{\text{hBest1}}$  (Andreeva et al., 2018).

The average molecular areas  $A_{\pi}$  obtained from the  $\pi/A$  isotherms of the mixed hBest1/POPC monolayers with different molar ratio of the two components match the calculated  $A_{\text{add}}$  values, indicating ideal mixing or complete phase separation. The fact that the  $\pi_{\text{col}}$  of POPC and binary hBest1/POPC monolayers (Figure 24A) match and that  $A_{\pi}$  follows the area additivity rule (Figure 25A) means that hBest1 and POPC are immiscible at the surface of the water subphase. Analysis of  $\pi/A$  isotherms by Goodrich's approach presents  $\Delta G_{\text{exc}}^{\pi}$  and  $\Delta G_{\text{mix}}^{\pi}$  of binary hBest1/POPC monolayers as a function of composition ( $X_{\text{hBest1}}$ ) at surface pressures of 10 and 20 mN/m (Figure 25B,C). It seems that the surface behavior of hBest1 and POPC in binary monolayers depends drastically on their molar ratio (corresponding to the area they occupy on the surface). Both the  $\Delta G_{\text{exc}}^{\pi}/X_{\text{hBest1}}$  and  $\Delta G_{\text{mix}}^{\pi}/X_{\text{hBest1}}$  dependences show positive free energies for the hBest1/POPC monolayers at 1:45 and 1:1 molar ratio and negative at 1:15 molar ratio. A stable monolayer is formed if  $\Delta G_{\text{exc}}^{\pi}$  is negative, i.e., at a molar ratio of 1:15. If  $\Delta G_{\text{exc}}^{\pi}$  is positive, the film is phase separated, i.e. all films at  $X_{\text{hBest1}} > 0.1$  (Figure 25A, B). The negative value of  $\Delta G_{\text{exc}}^{\pi}$  indicates the mutual attraction of the molecules in the binary monolayers and suggests that the influence of molecular interactions on the stability of the monolayer is more significant for the two-component monolayer with molar fraction  $X_{\text{hBest1}} = 0.067$ , compared to the monolayers with other compositions. Furthermore, the negative deviation of  $\Delta G_{\text{exc}}^{\pi}$  increases with increasing surface pressure (from -3.8 kJ/mol at 10 mN/m to -5.2 kJ/mol at 20 mN/m), implying that the intermolecular interactions are stronger when the binary monolayer exists in a more condensed state. All other hBest1/POPC monolayers showed positive  $\Delta G_{\text{mix}}^{\pi}$  values, suggesting the possibility of phase separation (immiscibility). The location of the maximum of  $\Delta G_{\text{mix}}^{\pi}$  at  $X_{\text{hBest1}} = 0.5$  indicates that equimolar mixing is thermodynamically the most unfavorable.

### 2.4.1. Effects of $\text{Ca}^{2+}$ , Glu and GABA on the morphology of hBest1/POPC Langmuir monolayers

We also carried out a study of the surface morphology of Langmuir monolayers, but containing not only protein but also lipid. Initial experiments were performed with POPC monolayers (**Figure 22**).

In the hBest1/POPC monolayers, after film relaxation, numerous voids and small oval domains of higher density, uniformly distributed in the surrounding homogeneous film, were observed (**Figure 26A**).

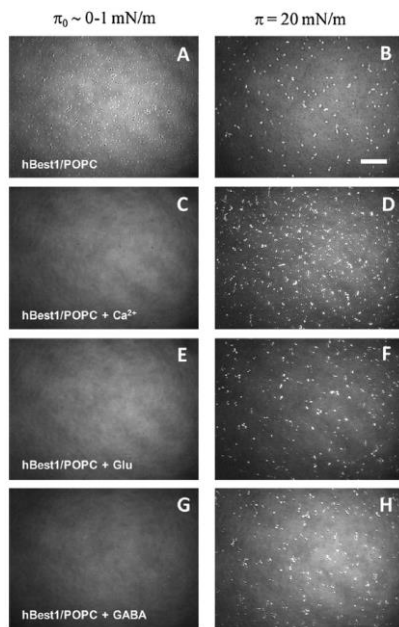


**Figure 26.** BAM images of composite hBest1/POPC (1/45) films on water substrates containing 150 mM NaCl (**A, B**) with addition of 0,5  $\mu\text{M}$   $\text{Ca}^{2+}$  (**C, D**), 2 mM Glu (**E, F**) and 100  $\mu\text{M}$  GABA (**G, H**), taken 30 min post spreading of uncompressed monolayers (left column) and at 20 mN/m (right column). The white bar represents 100  $\mu\text{m}$  (**Andreeva et al., 2018**).

In contrast, hBest1/POPC monolayers that contained  $\text{Ca}^{2+}$ , Glu or GABA were completely homogeneous (**Figure 26C, E, G**). Homogeneous gray areas, which contain uniformly distributed bright regions of different size but equal reflectivity, are observed when all composite films are compressed at 20 mN/m (**Figure 26, right column**). Since the reflectivity depends on the density of the monolayer, these aggregates are most likely made up of tightly packed POPC molecules. The largest number of such domains is observed in the presence of  $\text{Ca}^{2+}$ . As seen in (**Figure 22**), compression did not change the morphology of single component hBest1 films, but the morphology of POPC films in the presence of  $\text{Ca}^{2+}$ , Glu and GABA was significantly affected, proving the

predominant lipid composition of the domains and the phase separation of protein and lipid molecules in hBest1/POPC monolayers at higher surface pressure.

#### **2.4.2. Effects of $\text{Ca}^{2+}$ , Glu, and GABA on hBest1 topology in hBest1/POPC Langmuir-Blodgett films**

The hBest1/POPC films were visualized by AFM. We found that hBest1 increased its height and lateral dimensions and changed its compact oval shape (**Figure 23E–H**) (**Table 2**). The shape of the protein was more irregular, with one or two lower formations visible around the central oval protein body. The observed changes may be due to protein conformational dynamics and/or dimerization. These results raised the question of the presence of boundary POPC molecules (annular lipids) to cover the hydrophobic surface of hBest1, changing the shape, size and hydrophilicity of the protein, similar to cytochrome C oxidase (55 annular lipids) and rhodopsin (24 annular lipids).

We can summarize that  $\text{Ca}^{2+}$ , Glu, and GABA affect the properties of hBest1 in monolayers by changing the surface activity, size, topology, orientation, and organization of protein molecules at the air/water interface without significant effects on the  $\pi/A$  isotherms and hysteresis of the binary hBest1/POPC monolayers. The effects of  $\text{Ca}^{2+}$ , Glu, and GABA on the surface dynamics of hBest1 in binary monolayers were neutralized by POPC, so that the corresponding changes in protein morphology, topology, and orientation could be observed and detected by BAM and AFM. Binary films of hBest1 and POPC are immiscible at  $X_{\text{hBest1}} > 0.1$ , indicating that lipid-lipid and protein-protein interactions are stronger than lipid-protein interactions under conditions of their coexistence in the plane of the monolayer. This suggests that increasing the area (surface) occupied by protein molecules can have an impact on the possibility of protein oligomerization, the proper structuring and biological function of cell membranes.

These effects of  $\text{Ca}^{2+}$ , Glu, GABA and POPC on the native protein structure, conformation, surface organization and behavior of hBest1 affect not only its transport functions across biological membranes but also its interactions with other membrane channels, thus contribute to the maintenance of cellular homeostasis and proper cellular functioning.

#### **2.5. Effects of $\text{Ca}^{2+}$ , Glu and GABA on the $\pi/A$ isotherms and hystereses of hBest1/SM Langmuir monolayers**

Studies of the surface properties of hBest1 continued with binary Langmuir monolayers containing SM. We again analyzed the surface dynamics of hBest1 monolayers and SM monolayers containing  $\text{Ca}^{2+}$ , Glu, and GABA under physiological conditions. The effects of  $\text{Ca}^{2+}$ , Glu and GABA on SM monolayers at 35 °C are more complex.

For both hBest1/POPC and hBest1/SM, we used a ratio of 1:3 (area occupied by protein to that occupied by surrounding lipids) when constructing the Langmuir monolayers. We found that at 20 mN/m the surface area of one hBest1 molecule was 28.5 times higher than that of one SM molecule, which determined a molar ratio of 1:86 of the two components in the hBest1/SM monolayers. The  $\pi/A$  isotherms of the binary

hBest1/SM films on NaCl subphase as well as in the presence of  $\text{Ca}^{2+}$ , Glu and GABA show an identical course (trend) (**Figure 27A**) and are similar to the isotherms of SM monolayers.

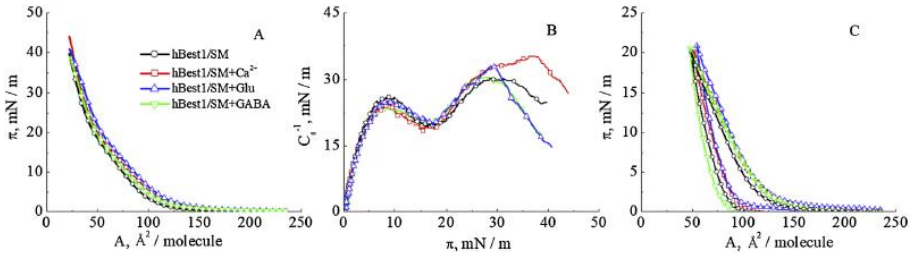


**Figure 27.** **A**) Surface pressure/mean molecular area ( $\pi/A$ ) isotherms; **B**) compressibility moduli,  $C_s^{-1}$ , versus surface pressure ( $\pi$ ) and **C**)  $\pi/A$  hysteresis loops of hBest1/SM monolayers at the air/water interface. The subphases contain 150 mM NaCl with addition of  $\text{Ca}^{2+}$ , Glu and GABA at  $35 \pm 2$  °C. (Mladenov et al., 2020).

Two regions with different slopes of the  $\pi/A$  curves are clearly distinguished, and the transition between them is at  $\pi_{tr} \sim 20$  mN/m. Again, the exact value of  $\pi_{tr}$  can be “derived” from the curves of compressibility moduli versus surface pressure ( $C_s^{-1}/\pi$ ). Two well-defined compressibility moduli maxima separated by a minimum at 17 mN/m are observed in **Figure 27B**. The compressibility moduli at both maxima are in the range of the LE phase ( $C_s^{-1} = 10 - 50$  mN/m), which means that the bicomponent hBest1/SM monolayers do not undergo a phase transition. The  $\pi_{tr}$  value was not affected by the addition of  $\text{Ca}^{2+}$ , Glu and GABA. The maximum compressibility moduli of the SM monolayers are in the range of  $50 \pm 3$  mN/m depending on the subphase composition, but the addition of hBest1 decreases the compressibility modulus of the SM monolayers, thus causing “fluidization” of the SM films and hindering the phase transition between the LE phase and the intermediate (M) phase (consisting of a mixture between the liquid-expanded and the condensed phase) (**Figure 27B**). We found that the  $\pi/A$  compression-decompression cycles of hBest1/SM monolayers (**Figure 27C**) showed the same trend as those of hBest1. The decompression curves were steeper and located at lower molecular areas than the compression ones, with significant hysteresis reaching 40% of the average molecular area.

The reason for this hysteresis is most likely the irreversible extrusion of the protein molecules into the aqueous phase during the compression of the films. The hysteresis values of hBest1/SM monolayers increased in the opposite order to that observed for hBest1 monolayers -  $\Delta A^{\text{GABA}} > \Delta A^{\text{Glu}} > \Delta A^{\text{NaCl}} > \Delta A^{\text{Ca}}$ , due to the larger molar fraction of SM in the studied binary films. The steeper increase in surface pressure of hBest1/SM monolayers over  $\pi_{tr}$  (**Figure 27C**) resembles the SM isotherms. Extrapolating these steep high-pressure parts, both SM and hBest1/SM isotherms to the abscissa show the same values of area per molecule at zero compression,  $A_0 = 60$   $\text{\AA}^2$ /molecule, indicating that only SM molecules are present on the film surface after  $\pi_{tr}$ .

For both hBest1/POPC and hBest1/SM monolayers, to investigate the miscibility of the monolayers, we observed (**Figure 28**) the deviation of the experimental average molecular areas  $A^\pi$  from the additivity rule (obtained from the  $\pi/A$  isotherms in **Figure 27A** at surface pressures of 5, 10 and 20 mN/m, all below  $\pi_{ir}$ ). Since the isotherms of hBest1<sup>Glu</sup> and hBest1<sup>GABA</sup> did not reach 20 mN/m, the  $A^\pi$  values at this surface pressure were not presented in **Figure 28**.

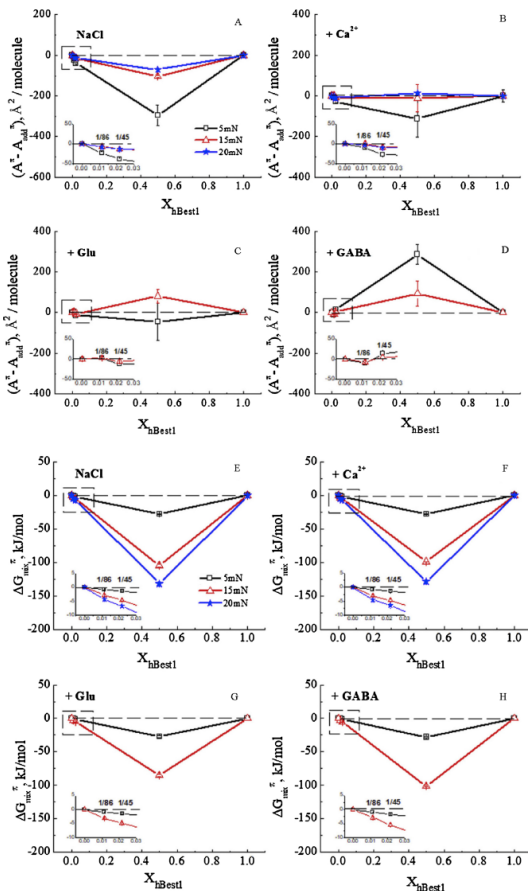


**Figure 28.** Plots of the deviation of the experimental molecular area  $A^\pi$  from the additive rule and total free energy of mixing versus composition (plots) for two component hBest1/SM monolayers on NaCl subphase (**A, E**) with addition of Ca<sup>2+</sup> (**B, F**), Glu (**C, G**) or GABA (**D, H**) at surface pressures of 5 mN/m, 15 mN/m and/or 20 mN/m. The insets represent a magnification of the framed areas. Data are represented as mean  $\pm$  SE (Mladenov et al., 2020).

The calculated theoretical molecular areas  $A_{\text{add}}^\pi$  correspond to either ideal mixing or complete phase separation of hBest1 and SM in the monolayers. The average areas  $A^\pi$  of hBest1/SM monolayers on a subphase containing NaCl showed a negative deviation from the additivity rule, regardless of the molar ratio of the two components (1:86, 1:45 and 1:1) (**Figure 28A**). These results indicate that intermolecular interactions between hBest1 and SM (in hBest1/SM monolayers) are stronger than hBest1-hBest1 or SM-SM intermolecular interactions, and at a 1:1 molar ratio, non-ideal molecular mixing is the most thermodynamically favorable (**Figure 28A**). As surface pressure increases,  $A^\pi$  values approach  $A_{\text{add}}^\pi$ , suggesting enhanced mixing or phase separation. The average molecular areas  $A_\pi$  of the hBest1/SM monolayers on the  $\text{Ca}^{2+}$ -containing subphase increased linearly with increasing hBest1 molar fraction, thus following additive lines at 15 and 20 mN/m (**Figure 28B**). In this case, the hBest1-SM intermolecular interactions are equalized to hBest1-hBest1 and SM-SM, which means ideal mixing or complete phase separation. In the presence of Glu, intermolecular hBest1-SM interactions dominate hBest1-hBest1 and SM-SM at low surface pressures, but weaken and become repulsive at 15 mN/m, as indicated by the positive deviation of the molecular regions from the additive line (**Figure 28C**). Addition of GABA also showed the tendency to separate protein and lipid molecules (**Figure 28D**), but this effect decreased with increasing surface pressure (Glu and GABA interact with the polar head of SM, leading to either repulsion between hBest1 and SM molecules, or incorporation of Glu and GABA into the binary monolayers).

Quantitative analysis and discrimination between ideal mixing and complete phase separation of hBest1 and SM in the binary monolayers was performed by applying the Goodrich approach to calculate the excess and total free energies of mixing  $\Delta G_{\text{exc}}^\pi$  and  $\Delta G_{\text{mix}}^\pi$ . Since the energy of ideal mixing is negligible compared to the excess free energy of mixing i.e. the values of  $\Delta G_{\text{exc}}^\pi$  and  $\Delta G_{\text{mix}}^\pi$  are approximately the same, so only  $\Delta G_{\text{mix}}^\pi$  was plotted in **Figure 28E–H**. The hBest1<sup>Glu</sup> and hBest1<sup>GABA</sup> isotherms do not reach 20 mN/m, therefore  $\Delta G_{\text{exc}}^\pi$  and  $\Delta G_{\text{mix}}^\pi$  cannot be calculated (at this  $\pi$ ) and are not plotted in **Figure 28G, H**. We found that the total free energy of mixing was not affected by the addition of  $\text{Ca}^{2+}$ , Glu, and GABA. The negative values of  $\Delta G_{\text{exc}}^\pi$  and  $\Delta G_{\text{mix}}^\pi$  suggest that the binary hBest1/SM monolayers are more stable than the hBest1 and SM monolayers and that the mixing process is spontaneous. Upon further compression of monolayers, the negative values of  $\Delta G_{\text{exc}}^\pi$  and  $\Delta G_{\text{mix}}^\pi$  increase, indicating that mixing and stability are improved, i.e. intermolecular interactions are stronger when the binary monolayers exist in a more condensed state and that equimolar mixing is thermodynamically the most favorable. In contrast, in studies with hBest1/POPC binary monolayers, we have shown that phase separation/mixing depends on the molar ratio of the components. Miscibility between hBest1 and SM most likely involves interactions with amide and hydroxyl groups of SM acting as hydrogen bond donors and acceptors, while phosphatidylcholine provides only hydrogen acceptors (ester carbonyl groups) for protein–lipid interactions. In conclusion, we can argue that **the miscibility of hBest1 and SM on the surface of monolayers is a fundamental physicochemical feature and is a prerequisite for strong protein-lipid interactions.**

### 2.5.1. Effects of $\text{Ca}^{2+}$ , Glu and GABA on the morphology of hBest1/SM Langmuir monolayers

Studies on the morphology of hBest1/SM monolayers were performed in parallel with studies on hBest1 and SM monolayers. BAM images of the binary hBest1/SM (1/86) monolayers show compact homogeneous film structures at 0 mN/m (before compression) and at 15 mN/m (**Figure 29**).

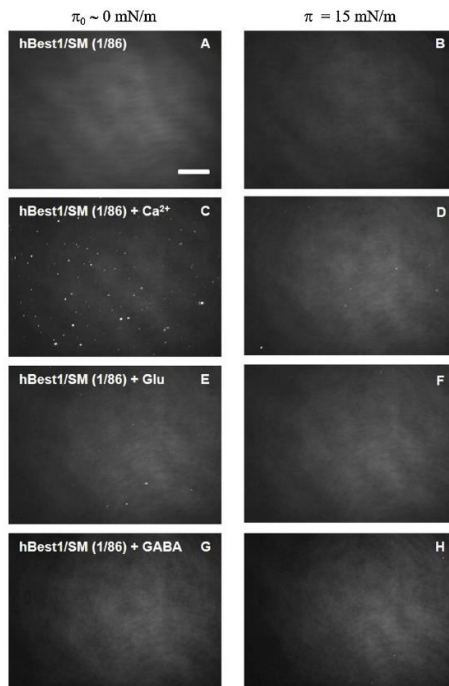


**Figure 29.** BAM images of uncompressed (left column) and compressed (right column) binary hBest1/SM (1/86) monolayers on liquid NaCl subphase (**A, B**), with addition of  $\text{Ca}^{2+}$  (**C, D**), Glu (**E, F**) and GABA (**G, H**). The white scale bar = 100  $\mu\text{m}$  (Mladenov et al., 2020).

No phase separation, domain formation or phase transition was observed. Addition of GABA has no impact on the morphology of the monolayers (**Figure 29G, H**). We found that the addition of  $\text{Ca}^{2+}$  provoked a partial phase separation of hBest1 and SM, with small, round, bright micrometer domains appearing after equilibration of the monolayers (**Figure 29C**). As the surface pressure increases, during compression, the number and size of the bright domains decrease and at 15 mN/m they completely disappear (**Figure 29D**). Addition of Glu resulted in separation of hBest1 and SM to a much lesser extent than  $\text{Ca}^{2+}$  - several less bright domains were observed at  $\pi \sim 0$  mN/m (**Figure 29E**) and disappeared upon compression to 15 mN/m (**Figure 29F**). These

observations are consistent with the results of thermodynamic analysis of miscibility, which showed that both mixing and intermolecular interactions in binary monolayers are enhanced with increasing surface pressure. We established that, in contrast to hBest1/SM monolayers,  $\text{Ca}^{2+}$  induced stronger protein-protein interactions, protein conformational changes, and macroorganization in hBest1/POPC monolayers.

In chapter 2.5. studies were focused on the interactions between hBest1 and SM, and the results clearly showed that in binary monolayers, hBest1 and SM mix spontaneously, which is a prerequisite determining the affinity between hBest1 and SM in the biological membranes. These results correspond well with the results obtained for the association of hBest1 with the lipid microdomains in the plasma membranes of MDCK II – hBest1 cells and determined the subsequent studies with the addition of cholesterol in the model membranes.

## **2.6. Surface properties of two- and three-component Langmuir monolayers containing cholesterol**

The liquid-ordered ( $L_o$ ) fractions in the cell membrane are enriched in sphingolipids and cholesterol and exist in a significantly more condensed state compared to the liquid-disordered ( $L_d$ ) fractions. In fact, one of the main properties of cholesterol is its condensing effect, which affects the structure and function of many proteins in biological membranes, including the membranes themselves. We found that cholesterol induced a condensing effect on monolayers containing hBest1, hBest1+SM, and hBest1+POPC, and confirmed the presence of such an effect on SM and POPC monolayers under the experimental conditions. We also showed that  $\text{Ca}^{2+}$  ions play a key role in realizing the condensing potential of cholesterol in monolayers. Therefore, we continued the study by characterizing the surface properties and surface dynamics of Langmuir monolayers containing cholesterol. In these studies, we used a bottom-up approach, i.e. we first investigated the less complex binary subsystems of POPC/Chol, SM/Chol, and hBest1/Chol as the basis for the more complex ternary systems hBest1/POPC/Chol and hBest1/SM/Chol.

### **2.6.1. Surface properties of cholesterol containing bicomponent monolayers**

( $\pi/A$ ) isotherms of binary monolayers POPC/Chol, SM/Chol and hBest1/Chol (presented in **Figures 30, 31 and 32**) show the gradual increase in surface pressure and molecular packing accompanying the decrease in average molecular area during compression, but with no indication of phase transitions (such as plateaus or curves).

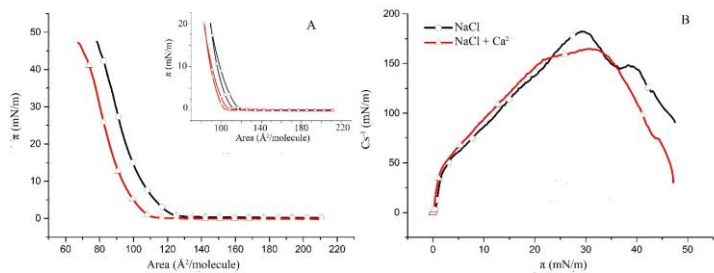


**Figure 30.** **A)** Surface pressure/mean molecular area isotherms of the binary POPC/Chol (1:1) monolayers in a subphase of 150 mM NaCl (black) and in 150 mM NaCl supplemented with 0.5  $\mu\text{M}$   $\text{CaCl}_2$  (red) at  $35 \pm 2^\circ\text{C}$  (inset:  $\pi/A$  hysteresis cycles of compression–decompression); **B)** surface compressibility moduli  $C_s^{-1}$  derived from the isotherms in **(A)** as a function of surface pressure (Videv et al., 2022).

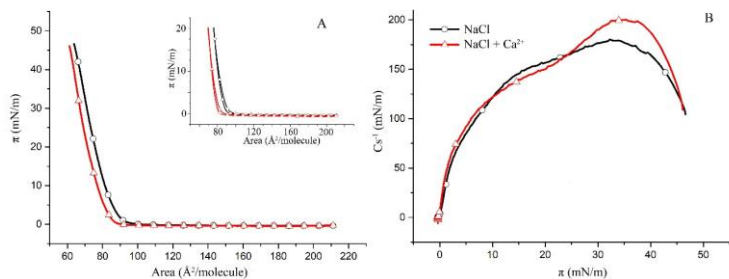


**Figure 31.** **A)** Surface pressure/mean molecular area isotherms of the binary SM/Chol (1:1) monolayers in a subphase of 150 mM NaCl (black) and in 150 mM NaCl supplemented with 0.5  $\mu\text{M}$   $\text{CaCl}_2$  (red) at  $35 \pm 2^\circ\text{C}$  (inset:  $\pi/A$  hysteresis cycles of compression–decompression); **B)** surface compressibility moduli  $C_s^{-1}$  derived from the isotherms in **(A)** as a function of surface pressure (Videv et al., 2022).

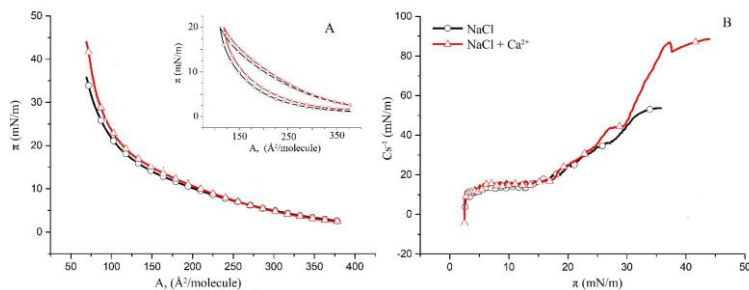


**Figure 32. A)** Surface pressure/mean molecular area isotherms of the binary hBest1/Chol (1:58,5) monolayers in a subphase of 150 mM NaCl (black) and in 150 mM NaCl supplemented with 0.5  $\mu\text{M}$   $\text{CaCl}_2$  (red) at  $35 \pm 2^\circ\text{C}$  (inset:  $\pi/A$  hysteresis cycles of compression–decompression); **B)** surface compressibility moduli  $C_s^{-1}$  derived from the isotherms in (A) as a function of surface pressure (Videv et al., 2022).

However, the three isotherms were different in shape and course. We found that the  $\pi/A$  compression isotherms of POPC/Chol and SM/Chol monolayers with the addition of  $\text{Ca}^{2+}$  shift to smaller molecular areas at a given  $\pi$ , compared to the isotherms without  $\text{Ca}^{2+}$ . The shape and slope of the isotherms for these monolayers do not change, indicating that the presence of  $\text{Ca}^{2+}$  does not affect either the phase state or their molecular organization. Other interesting features we observed in the  $\pi/A$  isotherms are the surface collapse pressure ( $\pi_{\text{col}}$ ) and the collapse area per molecule ( $A_{\text{col}}$ ). While  $\pi_{\text{col}}$  was not affected by the addition of  $\text{Ca}^{2+}$ ,  $A_{\text{col}}$  (a measure of the condensing effect of  $\text{Ca}^{2+}$ ) decreased by  $10 \text{ \AA}^2/\text{molecule}$  in POPC/Chol monolayers (Figure 30A) and only  $4 \text{ \AA}^2/\text{molecule}$  in SM/Chol monolayers. The condensing effect of  $\text{Ca}^{2+}$  is also reflected in the reduction of hysteresis of POPC/Chol (Figure 30A, inset) and SM/Chol (Figure 31A, inset) monolayers, again this effect is stronger in the first model system. The hysteresis of monolayers results from the hydrophilic-lipophilic balance obtained in the interaction between lipid molecules, molecular cohesion and the interaction between the polar head and the subphase, which determine the molecular packing and viscoelastic properties of the monolayers at the surface during compression and decompression. Essentially, the addition and binding of  $\text{Ca}^{2+}$  affects each of these parameters, and the balance between them upon monolayer compaction alters the reversibility of the molecular reorganizations occurring during the compression and decompression of monolayers. Through a combination of experimental ( $\pi/A$  isotherms) and theoretical (molecular dynamics simulations) studies, we have shown that the addition of  $\text{Ca}^{2+}$  does not change the shape of the  $\pi/A$  isotherms of Chol, but shifts them to a significantly lower mean molecular area.

In our studies, we found no noticeable effect of  $\text{Ca}^{2+}$  on POPC monolayers at a  $\text{Ca}^{2+}$  concentration of  $0.5 \mu\text{M}$ , which means that the condensing effect of  $\text{Ca}^{2+}$  on binary POPC/Chol monolayers mainly originates from the effect on Chol molecules.

Both maxima of the  $C_s^{-1}$  compressibility moduli in POPC/Chol monolayers (without and with  $\text{Ca}^{2+}$  in the subphase) (Figure 30B) are in the range (from 100 to 250

mN/m) characteristic of a liquid-condensed phase.  $C_s^{-1}$  is virtually unaffected by  $Ca^{2+}$  addition, with maximum values of  $C_s^{-1}$  decreasing by only 15 mN/m and shifting to a slightly higher surface pressure.

The maximum compressibility moduli of the SM/Chol monolayers presented in **Figure 31B** indicate that the monolayers are in the same liquid-condensed (LC) phase. The maximum  $C_s^{-1}$  in this case increases by about 20 mN/m and also shifts to a slightly higher surface pressure. The shift to higher  $\pi$  suggests a slight stabilization “promoted” by  $Ca^{2+}$  in these binary monolayers. A characteristic feature of SM monolayers is the LE-LC phase transition, which is manifested by a broad plateau (at a surface pressure of 6 to 15 mN/m) on the  $C_s^{-1}/\pi$  graph. A similar plateau is absent in SM/Chol monolayers, suggesting molecular mixing of molecules from both lipids. The maximum compressibility modulus of SM monolayers at 35°C is about 50 mN/m. Addition of Chol at a 1:1 molar ratio causes a 3.5- and fourfold increase in this value, respectively, thereby changing the phase state from LE to LC.

For the binary hBest1/Chol monolayers, two distinct regions were distinguished in the  $\pi/A$  isotherms (molar ratio 1:58.5, corresponding to a surface area ratio of 1:3) (**Figure 32**). At low surface pressures up to about 20 mN/m, the isotherm resembled that of pure hBest1, while at higher surface pressures it appeared similar to that of Chol. Both isotherms show identical shapes and an initial surface pressure of  $\pi_0 = 2.6$  mN/m, which coincide with each other to  $\pi \sim 13$  mN/m. Above 13 mN/m, the  $Ca^{2+}$  added hBest1/Chol isotherms shift to slightly higher molecular areas in contrast to the POPC/Chol and SM/Chol monolayers, which shift to lower areas.

Cholesterol monolayers on different aqueous and buffer subphases and temperature conditions have been studied by different scientific groups. We found that upon addition of hBest1 the maximum compressibility modulus of the Chol monolayer ( $C_s^{-1}max$ ), which was reached at  $\pi$  35 mN/m, was 53 mN/m (**Figure 32B**), while with a monolayer of cholesterol molecules alone it was over 300 mN/m, indicating that the monolayers become more disordered. However, the addition of  $Ca^{2+}$  improved the order of the molecules in the hBest1/Chol monolayer, due to increased values of  $C_s^{-1}$  (max)  $\sim 90$  mN/m. In contrast, the maximum  $C_s^{-1}$  of hBest1/Chol monolayers without and with  $Ca^{2+}$  was fourfold and eightfold higher, respectively, compared to pure hBest1 films, suggesting a strong decrease in the elasticity and fluidity of the protein film, which is related to the condensing role of Chol and Chol+ $Ca^{2+}$ . The  $\pi/A$  compression-decompression cycles of the hBest1/Chol monolayers (**Figure 32A, inset**) confirmed that the addition of hBest1 reduced the molecular ordering and increased the fluidity of the Chol monolayer. The Chol monolayer showed almost zero hysteresis, but when hBest1 was added, the hysteresis became significant and similar to that of the hBest1 and hBest1/POPC monolayers. The shape of the compression-decompression cycles, as well as the magnitude of the hysteresis, were not affected by the presence of  $Ca^{2+}$ .

### 2.6.2. Surface properties of ternary monolayers containing hBest1 and cholesterol

These studies are key to investigating the surface organization of hBest1 and cholesterol containing monolayers, as we simulated the surface characteristics of the

more disordered and more ordered microdomains in biological membranes using the hBest1/POPC/Chol and hBest1/SM/Chol monolayers.

In constructing the binary hBest1/POPC and hBest1/SM films, the hBest1:lipid area ratio was 1:3 (the area of the monolayer occupied by proteins to the area occupied by lipids). To investigate the thermodynamic behavior of ternary hBest1/POPC/Chol and hBest1/SM/Chol systems under biologically relevant conditions, we used the same area ratio of 1:3 that we achieved at molar ratios of 1:45:45 and 1:86:86, respectively, by maintaining an equimolar ratio (1:1) between the two lipids.

We found that the addition of hBest1 protein molecules completely changed the  $\pi/A$  isotherm of the binary lipid POPC/Chol monolayer. In fact, the shape of the isotherm is more like that of the hBest1/Chol monolayer. The  $\pi/A$  isotherms of hBest1/POPC/Chol monolayers have identical shapes, as "stretched" sinusoidal curves in the absence and presence of  $\text{Ca}^{2+}$  (**Figure 33A**).

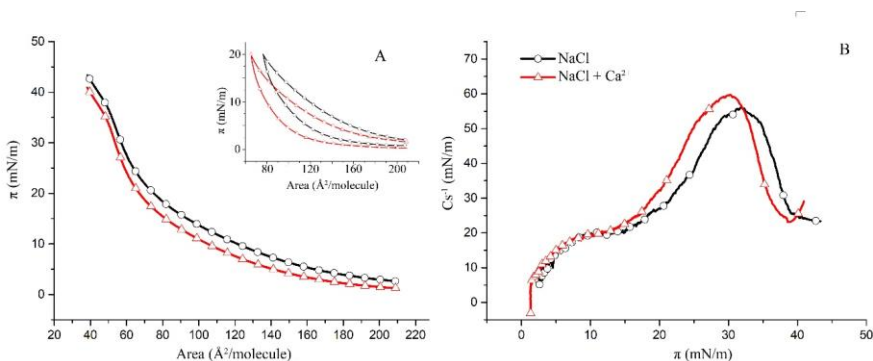


**Figure 33. A)** Surface pressure/mean molecular area isotherms of the ternary hBest1/POPC/Chol (1:45:45) monolayers in a subphase of 150 mM NaCl (black) and in 150 mM NaCl supplemented with 0.5  $\mu\text{M}$   $\text{CaCl}_2$  (red) at  $35\pm 2^\circ\text{C}$  (inset:  $\pi/A$  hysteresis cycles of compression–decompression); **B)** surface compressibility moduli  $C_s^{-1}$  derived from the isotherms in (A) as a function of surface pressure (**Videv et al., 2022**).

Upon addition of  $\text{Ca}^{2+}$ , we found a decrease in  $\pi_0$  from 2.6 mN/m to 1.3 mN/m, and the entire isotherm shifted to lower surface pressures, demonstrating the condensing effect of  $\text{Ca}^{2+}$  on the surface molecular organization. A change in the course of the isotherm is observed at about 15 mN/m ( $\pi_{\text{tr}}$ ).

The exact values of  $\pi_{\text{tr}}$  were determined from the  $C_s^{-1}/\pi$  curves (**Figure 33B**). The curves show a gradual increase in the compressibility modulus at low surface pressures below 13 mN/m ( $\pi_{\text{tr}}$ ), which is followed by a much steeper increase in  $C_s^{-1}$  at surface pressures from 13 mN/m to 32 mN/m (for the subphase without  $\text{Ca}^{2+}$ ) or 30 mN/m (for the subphase with  $\text{Ca}^{2+}$ ), where the maximum values of  $C_s^{-1}$  are reached.  $C_s^{-1}(\text{max})$  for the monolayer with the NaCl subphase is 56 mN/m, while for the monolayer with the NaCl subphase supplemented with  $\text{CaCl}_2$  is 60 mN/m, values that are slightly above the upper limit of 50 mN/m for the LE phase. These values are higher than the  $C_s^{-1}(\text{max})$  of hBest1 monolayers (10.7 mN/m) and significantly lower than the  $C_s^{-1}(\text{max})$

of POPC (~110 mN/m) and of Chol (839 mN/m), which is an indication of mixing of the three components of the monolayer. **The preservation of the LE phase state of the hBest1/POPC/Chol monolayer as well as the reduced value of  $\pi_{\text{col}}$  are an indication of a very good mixing of the monolayer components.**

The isotherm slopes of hBest1/SM/Chol monolayers are steeper than those of hBest1/POPC/Chol, therefore they are in a more condensed phase state. This also affected the surface elasticity of the films, which was expressed by the compressibility modulus (Figure 34A and B).

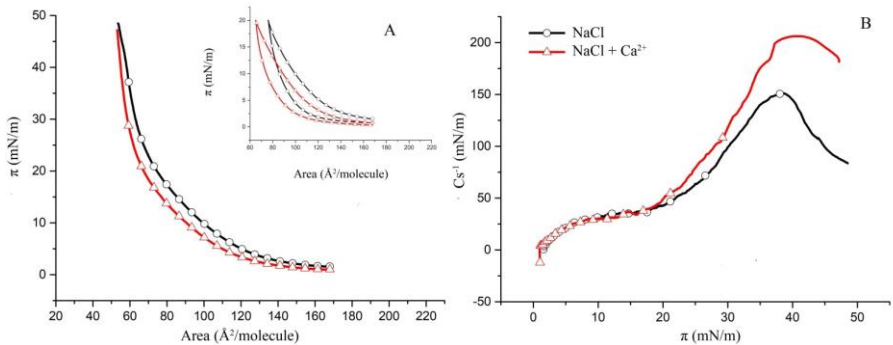


**Figure 34. A)** Surface pressure/mean molecular area isotherms of the binary hBest1/SM/Chol (1:86:86) monolayers in a subphase of 150 mM NaCl (black) and in 150 mM NaCl supplemented with 0.5  $\mu\text{M}$  CaCl<sub>2</sub> (red) at 35 $\pm$ 2 $^\circ\text{C}$  (inset:  $\pi/A$  hysteresis cycles of compression–decompression); **B)** surface compressibility moduli  $C_s^{-1}$  derived from the isotherms in (A) as a function of surface pressure (Videv et al., 2022).

The  $C_s^{-1}(\text{max})$  of the hBest1/SM/Chol monolayer in the absence of Ca<sup>2+</sup> is 152 mN/m, and in the presence of Ca<sup>2+</sup> it is 206 mN/m, which are 2.7 and 3.5 times higher than the values of hBest1/POPC/Chol monolayers and correspond to the LC phase state. These results indicate that Ca<sup>2+</sup> exerts a significant condensing and stabilizing effect on the hBest1/SM/Chol monolayers, due to the decrease in the elasticity of the films. Cholesterol is known to form highly condensed monolayers in the solid (S) phase state, with  $\pi_{\text{col}} \sim 45$  mN/m. None of the monolayers we examined showed the existence of an S phase state, therefore the Chol molecules were well mixed with the other components. In comparison, molecules in hBest1 monolayers (without and with Ca<sup>2+</sup>) self-assemble on the surface into an expanded monolayer at the air/water interface during compression without collapsing. The POPC monolayer was also in the LE phase state until collapsing at 46 mN/m.

The maximum  $C_s^{-1}$  values we found for hBest1/SM/Chol (1:86:86) monolayers were significantly higher than the  $C_s^{-1}(\text{max})$  of hBest1 monolayers (10.7 mN/m) and lower than the  $C_s^{-1}(\text{max})$  of SM (~220 mN/m) and Chol (839 mN/m) monolayers, which is a clear indication that the three components of these monolayers are mixed. SM (16:0), which was used in this study, underwent a LE-LC phase transition at a surface pressure of  $\pi_{\text{tr}} = 46.8$  mN/m, with both NaCl and NaCl + Ca<sup>2+</sup> in the subphases. This

effect disappeared when combined with hBest1 and Chol, again **supporting the statement that the components are mixed.**

## 2.7 Miscibility and phase separation in hBest1/POPC/Chol and hBest1/SM/Chol monolayers

To proceed with the thermodynamic analysis of the degree of miscibility between hBest1 and lipids (POPC, SM, and Chol) in the ternary monolayers, we constructed isotherms with different hBest1/lipid molar ratios as follows: 1:86:86 ( $X_{\text{hBest1}} = 0.006$ ); 1:58.5:58.5 ( $X_{\text{hBest1}} = 0.0085$ ); 1:45:45 ( $X_{\text{hBest1}} = 0.011$ ); 1:10:10 ( $X_{\text{hBest1}} = 0.048$ ); 1:2:2 ( $X_{\text{hBest1}} = 0.20$ ); 1:1:1 ( $X_{\text{hBest1}} = 0.33$ ), keeping the equimolar ratio between the two lipids as in the isotherms presented in Section 2.6.2. Based on the isotherms, both qualitative ( $\Delta A$ ) and quantitative ( $\Delta G_{\text{mix}}$ ) parameters of interactions between protein and lipid molecules were calculated. In **Figures 35 and 36**,  $\Delta A$  and  $\Delta G_{\text{mix}}$  are plotted as a function of hBest1 ( $X_{\text{hBest1}}$ ) molar fractions. The deviation  $\Delta A$  ( $A_{\text{exp}} - A_{\text{add}}$ ) in the average experimental molecular areas  $A_{\text{exp}}$  (obtained from the  $\pi/A$  isotherms of hBest1/POPC/Chol and hBest1/SM/Chol monolayers) from the additive molecular areas ( $A_{\text{add}}$ ) and calculated from the additivity rule is a parameter, revealing the intermolecular interactions between the components of the monolayer (see 2.4.). The area deviations of hBest1/POPC/Chol and hBest1/SM/Chol monolayers that were formed in the absence and presence of  $\text{Ca}^{2+}$  at four different  $\pi$  but below  $\pi_{\text{tr}}$  are presented in **Figure 35A,B** and **Figure 36A,B**, respectively.

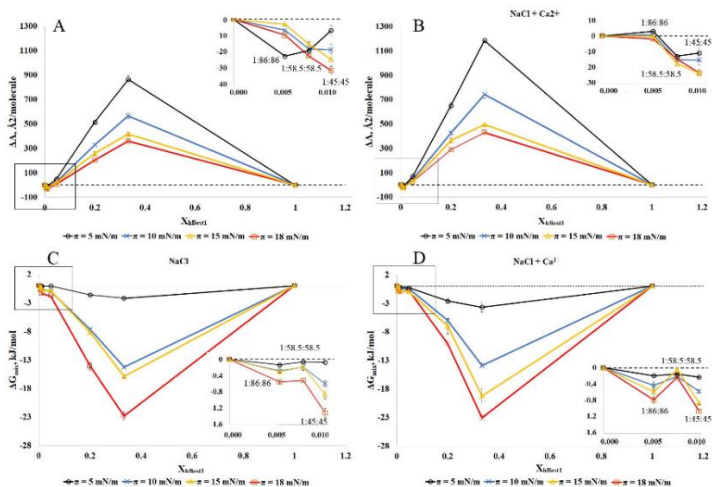


**Figure 35.** Plots of the deviation of the area from the additivity ( $\Delta A$ ) (**A**, **B**) and the total free energy of mixing ( $\Delta G_{\text{mix}}^T$ ) (**C**, **D**) versus film composition ( $X_{\text{hBest1}}$ ) at different surface pressures of hBest1/POPC/Chol monolayer in a subphase of 150 mM NaCl (**A**, **C**) and in 150 mM NaCl supplemented with 0.5  $\mu\text{M}$   $\text{CaCl}_2$  (**B**, **D**) at  $35 \pm 2^\circ\text{C}$  (inset: enlargement of the framed area) (Videv et al., 2022).

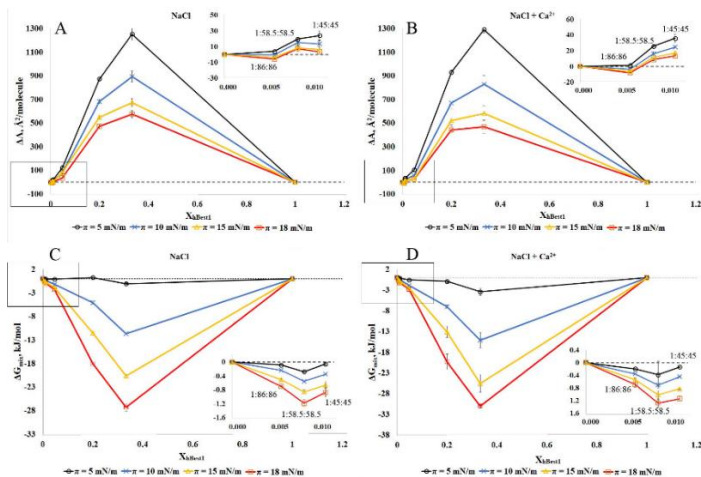


**Figure 36.** Plots of the deviation of the area from the additivity ( $\Delta A$ ) (**A**, **B**) and the total free energy of mixing ( $\Delta G_{\text{mix}}^{\text{T}}$ ) (**C**, **D**) versus film composition ( $X_{\text{hBest1}}$ ) at different surface pressures of hBest1/SM/Chol monolayer in a subphase of 150 mM NaCl (**A**, **C**) and in 150 mM NaCl supplemented with 0.5  $\mu\text{M}$   $\text{CaCl}_2$  (**B**, **D**) at  $35 \pm 2$  °C (inset: enlargement of the framed area) (Videv et al., 2022).

$\Delta A$  of hBest1/POPC/Chol monolayers (regardless of  $\pi$  and the presence of  $\text{Ca}^{2+}$ ) have negative or zero values at  $X_{\text{hBest1}} < 0.02$ , which correspond to biologically relevant conditions in cell membranes, and positive values at  $X_{\text{hBest1}} > 0.02$  (**Figure 35A, B**, insets). The  $\Delta A$  values in the hBest1/SM/Chol monolayers were positive, except for that at  $X_{\text{hBest1}} = 0.006$ , which “oscillates” around zero (**Figure 36A,B**, insets). The negative values suggest that in hBest1/POPC/Chol monolayers, the attractive interactions (forces) between hBest1 and lipid molecules are stronger than the protein–protein and lipid–lipid interactions, thus compacting the films and the miscibility between hBest1 and lipids increases. The positive  $\Delta A$  values in the films result from the stronger attraction between similar hBest1–hBest1 and lipid–lipid molecules, as well as the stronger repulsion between hBest1 and lipids, suggesting phase separation between hBest1 and lipids in the monolayers.

Values of  $\Delta A$  that are on the additive line define similar interaction strengths between all molecules, suggesting mixing or complete phase separation of the components of the monolayers. The higher the protein content, the higher the positive deviation from ideal mixing and the probability of phase separation of the components. This deviation is most pronounced at low  $\pi$ . The compaction of the monolayers was accompanied by an increase in  $\pi$ , which significantly reduced the deviation of the experimental molecular areas from the additive ones, suggesting a better mixing of the components. Addition of  $\text{Ca}^{2+}$  increased  $\Delta A$ , indicating better separation compared to the monolayer in the absence of  $\text{Ca}^{2+}$ .

To analyze the  $\pi/A$  isotherms of these two ternary monolayers, we again used the Goodrich's method. To calculate the total free energy of mixing  $\Delta G_{\text{mix}}^\pi$ , **we assumed that the monolayers were bicomponent**, in which one of the components was hBest1 and the other was a lipid mixture of POPC/Chol and SM/Chol. We used this approach because: 1) the Goodrich's method was obtained for a two component system and 2) equimolar POPC/Chol and SM/Chol monolayers are known to be very stable, have high affinity and "favorable" positioning between the two types of lipid molecules, which allowed us to investigate the effect of incorporating hBest1 into these binary lipid monolayers.

The negative  $\Delta G_{\text{mix}}^\pi$  values of hBest1/POPC/Chol and hBest1/SM/Chol monolayers indicate that the ternary monolayers are more stable than the single component hBest1 and lipid monolayers, implying **that the mixing of hBest1 and lipid molecules is a spontaneous and thermodynamically favorable process**. Mixing improved with increasing molar fraction of hBest1 and  $\pi$ , but was little affected by the addition of  $\text{Ca}^{2+}$  (**Figures 35C, D and 36C, D**). We have already shown the phase separation between POPC and hBest1 and the spontaneous mixing between SM and hBest1 in the hBest1/POPC and hBest1/SM binary monolayers. The results in section 2.7. showed that the effect of cholesterol on miscibility/phase separation in ternary films is very strong. **Cholesterol improved miscibility and stability in hBest1/POPC/Chol films by reducing the phase separation between hBest1 and POPC, while in hBest1/SM/Chol films miscibility was preserved, maintained and stabilized, albeit with increasing values of  $\Delta G_{\text{mix}}^\pi$ .**

The equilibrium and stabilization in the miscibility/phase separation between hBest1 and POPC/Chol on the one hand, between hBest1 and SM/Chol on the other, has a direct effect on the association and localization of the protein with lipid rafts, its conformation, surface organization and its functions.

## **2.8. Summary of results obtained from studies of hBest1 in models of biological membranes**

- These studies started with the establishment and optimization of a scheme to obtain purified hBest1 from MDCK II - hBest1 cells. We achieved a hBest1 yield of around 2.8%. **This was the second most important step in the studies with hBest1** because it allowed us to obtain the protein in a pure form for study.

- We found that 51.1% helical structural elements, including large and short  $\alpha$ -helices (total 23.9%) and  $3_{10}$  helices (27.2%) are involved in the secondary structure composition of hBest1. The addition of  $\text{Ca}^{2+}$  caused: an **increase** in all helical structures to 59.2%, mainly due to an increase in the content of  $\alpha$ -helices (by 5.6%); **reduction** of  $\beta$ -turns and loops up to 27.2% (in favor of helices); **reduction** of aggregated and antiparallel sheets from 16.7% to 13.6%.

- We found that in Langmuir monolayers of hBest1, the smallest possible area per molecule,  $A_0$ , for hBest1<sup>Glu</sup> and hBest1<sup>GABA</sup> is similar to that of the hBest1 monolayer ( $A_0 = 3700 \text{ \AA}^2/\text{monomer}$ ) and significantly smaller for hBest1<sup>Ca2+</sup> ( $A_0 = 3360 \text{ \AA}^2/\text{monomer}$ ).

- We found that the maximum compressibility moduli of hBest1 monolayers ( $C_s^{-1}(\text{max}) = 10.7 \text{ mN/m}$  for hBest1 and hBest1Ca<sup>2+</sup> and  $C_s^{-1}(\text{max}) = 11.8 \text{ mN/m}$  for hBest1<sup>Glu</sup> and hBest1<sup>GABA</sup>) are in the lower boundary for LE lipid films (ranging from 12.5 to 50 mN/m).
- We have shown that hBest1 monolayers (as well as with added Ca<sup>2+</sup>, Glu, and GABA) have significant hysteresis that decreases with increasing  $\pi$ .
- Based on the BAM images, we showed that the monolayers of hBest1, hBest1<sup>Ca2+</sup>, hBest1<sup>Glu</sup>, and hBest1<sup>GABA</sup> have different packing densities that are consistent with the results of the  $\pi/A$  isotherms.
- Based on AFM images of Langmuir–Blodgett films, we found that the hBest1 molecules have an oval shape, with lateral dimensions of  $100 \times 160 \text{ \AA}$  and a height of  $75 \text{ \AA}$ . Ca<sup>2+</sup>, Glu and GABA change the conformation of hBest1, but only Ca<sup>2+</sup> induces protein aggregation (dimerization and trimerization).
- We found that hBest1 exerts a "fluidizing" effect on POPC monolayers, whereby hBest1/POPC films exhibit increased elasticity.
- We showed that in hBest1/POPC films, POPC eliminated the effects of Ca<sup>2+</sup>, Glu, and GABA that were observed in hBest1 monolayers.
- We showed that  $\Delta G_{\text{exc}}^{\pi}/X_{\text{hBest1}}$  and  $\Delta G_{\text{mix}}^{\pi}/X_{\text{hBest1}}$  had negative values for hBest1/POPC monolayers with a 1:15 lipid:protein molar ratio and positive values for monolayers with 1:45 and 1:1 molar ratios, implying that hBest1 and POPCs are immiscible at the surface of the aqueous subphase.
- By AFM, we visualized the hBest1/POPC films. We found that hBest1 increases its height and lateral dimensions and changes its compact oval shape in the presence of Ca<sup>2+</sup>, Glu, and GABA.
- We showed that the addition of hBest1 decreased the compressibility modulus of SM monolayers, thereby inducing "fluidization" of hBest1/SM films.
- We found that the miscibility of hBest1 and SM at the surface of monolayers is a thermodynamically favorable process that is a fundamental physicochemical feature and a prerequisite for strong protein-lipid interactions.
- We found that cholesterol induced a condensing effect in monolayers containing hBest1, hBest1+SM, and hBest1+POPC.
- We found that hBest1/POPC/Chol and hBest1/SM/Chol films, regardless of the experimental conditions, showed negative values of  $\Delta G_{\text{mix}}^{\pi}$ , which means that the mixing of hBest1 and lipid molecules on the subphase surface is a spontaneous and thermodynamically favorable process
- We found that cholesterol enhanced and stabilized the mixing between the components in hBest1/POPC/Chol and hBest1/SM/Chol films, despite of the experimental conditions.

### 3. hBest1 and nanobiotechnology

The results of hBest1 behavior studies obtained through cell cultures and through model membranes provide the necessary fundamental knowledge for the application of

innovative therapies using nanostructures representing spherical nucleic acids as well as bilayer polymer-lipid discs, liposomes and bicontinuous structures or polymer nanoparticles to intercalate hBest1 into the cell membrane and restore its transport functions.

Here, we present the biological characterization of spherical nucleic acids constructed from a nonphospholipid nucleolipid, which is an original hybrid biomacromolecule composed of a hydrophobic residue similar to naturally occurring phospholipids and a DNA oligonucleotide chains (**Figures 37 and 38**).

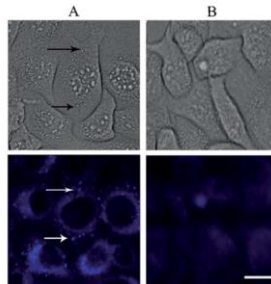


**Figure 37.** White light (up) and fluorescent (low) images of A549 cells following 30 min exposure to DPPC/Chol/NucL2 vesicles (**panel A**). The vesicles taken up by the cells are indicated by arrows. Imaging results with A549 cells that have not been treated with the vesicles (control) are shown in **panel B**. Scale bar 15  $\mu\text{m}$  applies for all images (**Dimitrov et al., 2022a**).

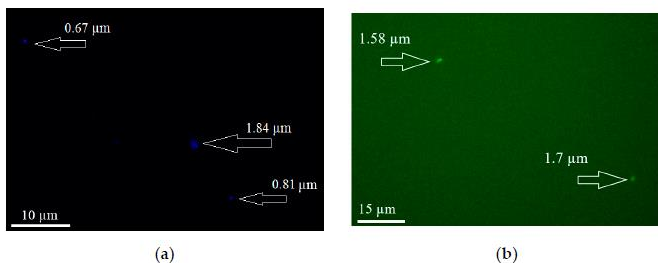


**Figure 38.** Fluorescent labeling of vesicular SNAs with (a) laurdan and (b) FITC (**Dimitrov et al., 2022b**).

No data on nanostructures loaded with hBest1 has been found in the literature (because so far there is no data of another team that has isolated and purified it), the realization of which is an experimental and scientific challenge for our scientific team, as they will provide valuable information about the structure and the mechanism of action of hBest1 in cells, as well as will reveal the potential of nanobiotechnology for biomedical applications.

## IV. Conclusions

1. Epithelial cells of the MDCK II line are a good model to study hBest1 sorting because they polarize in only about five days and have a very well defined apical and basolateral membrane.
2. Cells of the MDCK II line transcribe the *BEST1* gene but do not translate the hBest1 protein. After transfection in these cells, hBest1 was expressed and localized to the basolateral membrane, as in RPE cells.
3. Disturbances in the composition and structure of the potential basolateral sorting motifs Y85VTL, Y97ENL and Y227DWI, which are responsible for the clinical manifestations in BVMD patients, may cause incorrect sorting and localization of hBest1 mutant forms. Phosphorylation of hBest1 at Tyr 227 affects basolateral localization of the protein.
4. In cells of the stable MDCK II - hBest1 cell line, growth characteristics, metabolic activity, morphology, and polarization were not affected by stable hBest1 protein expression.
5. The hBest1 protein in MDCK II cells - hBest1 affects transepithelial resistance by delaying peak values. Addition of Glu and GABA increased TER values, while ATP decreased them.
6. MDCK II - hBest1 cells are more resistant to the enzymatic action of PLA<sub>2</sub>, most likely due to the increased amount of non-lamellar lipids compared to lamellar lipids in the cell membranes.
7. An increase in L<sub>d</sub> domains was observed in plasma membranes of MDCK II - hBest1 cells compared to L<sub>d</sub> domains in untransfected MDCK II cells. hBest1 localizes and self-assembles mainly in the L<sub>d</sub> domains (about 60-65%) of cell membranes, compared to 30-35% in the L<sub>o</sub> domains (lipid rafts).
8. About 51% helical structural regions are included in the secondary structure of hBest1, but the addition of Ca<sup>2+</sup> causes an increase in all helical structures to 59%.
9. hBest1 molecules have an oval shape, with lateral dimensions of 100 × 160 Å and a height of 75 Å. Ca<sup>2+</sup>, Glu and GABA change the conformation of hBest1, but only Ca<sup>2+</sup> can induce molecular aggregation.
10. The smallest possible area per molecule, A<sub>0</sub>, for hBest1<sup>Glu</sup> and hBest1<sup>GABA</sup> is similar to that of the hBest1 monolayer (A<sub>0</sub> = 3700 Å<sup>2</sup>/monomer) and significantly smaller for hBest1<sup>Ca<sup>2+</sup></sup> (A<sub>0</sub> = 3360 Å<sup>2</sup>/monomer).

11. Monolayers of hBest1, hBest1Ca<sup>2+</sup>, hBest1<sup>Glu</sup>, and hBest1<sup>GABA</sup> have different packing densities and C<sub>s</sub><sup>-1</sup> (max) values are at the lower limit for LE lipid films.
12. POPC abolished the effects of Ca<sup>2+</sup>, Glu, and GABA in hBest1/POPC films.
13. At physiological protein:lipid surface area ratios (1:3), hBest1 and POPC are immiscible.
14. In hBest1/POPC films, hBest1 molecules increase their height and lateral dimensions and change their compact oval shape upon addition of Ca<sup>2+</sup>, Glu, and GABA.
- 14 Monolayers of hBest1, hBest1<sup>Ca2+</sup>, hBest1<sup>Glu</sup>, and hBest1<sup>GABA</sup> have different packing densities.
15. hBest1 induces “fluidization” of the POPC and SM films.
16. The miscibility of hBest1 and SM on the surface of the monolayers is a spontaneous and thermodynamically favorable process despite of the experimental conditions.
17. Cholesterol induces a condensing effect on monolayers containing hBest1, hBest1+SM and hBest1+POPC.
18. Mixing of hBest1 molecules and lipids in hBest1/POPC/Chol and hBest1/SM/Chol monolayers is also a spontaneous and thermodynamically favorable process. Cholesterol enhances and stabilizes the mixing between the components.

In conclusion, the results of our long term studies show that the correct localization of hBest1 on the basolateral membrane of cells depends on the participation of at least three sorting signals, and changing the amino acid composition of each signal individually cannot "reverse" the localization of the protein on the apical membrane, but causes only a partial change in this direction. Therefore, it is more correct to assume a cumulative effect of several sorting signals to achieve the complete reversal of hBest1 localization. But even the partial apical localization of the protein and the increase in the number of hBest1 molecules on the apical membrane disrupts ion transport through the cells of the retinal pigment epithelium, increasing the concentration of anions in the space around the photoreceptors, and this gradually can lead to their damage and death, which over the time causes progressive vision loss.

Using PLA<sub>2</sub> and TER, we indirectly but “elegantly” showed that altered metabolism by hBest1 towards the synthesis and/or accumulation of non lamellar lipids, reduced the effect of PLA<sub>2</sub> on MDCK II - hBest1 cells, as TER changed very little (below 10%). However, even with the reduced enzymatic action of PLA<sub>2</sub> on cells, the liquid-ordered phase increases and the liquid-disordered phase decreases in cell membranes, where hBest1 is mainly localized (about 70% in L<sub>d</sub>), which determines the inactivation of the channel in the liquid-ordered phase.

Extensive studies with monolayers containing hBest1 and major lipids, including cholesterol, revealed the interaction forces between the various molecules, ie. the presence of miscibility or phase separation at the surface of the films, which prompted subsequent research with nanoparticles.

## V. Contributions

### Contributions of fundamental value

1. Large scale studies performed with biological membrane models contributed to a deep understanding of the molecular mechanisms of interaction of hBest1 with major lipids, determining the surface properties, localization, (self)organization and functions of hBest1 in cell membranes.

2. Elements of the secondary structure of hBest1 and the influence of  $\text{Ca}^{2+}$  on its conformation were determined.

3. Changes in lipid composition in the membranes of MDCK II cells induced by hBest1 were determined.

### Contributions of scientific and applied value

1. Two new hBest1 stably transfected cell lines were established: RPE1-hBest1 derived from retinal pigment epithelium and MDCK II-hBest1 derived from renal epithelium. All previously established cell lines that even endogenously express hBest1 lose their translation when the cells are incubated *in vitro*.

2. hBest1 was purified and isolated from the cells of the newly established cell line MDCK II - hBest1, which determined the possibility of conducting all subsequent studies with model membranes and nanoparticles.

### Contributions of methodological value

1. The miscibility of hBest1 in two-component monolayers was determined by an original application of Goodrich's method to find  $\Delta A$  and  $\Delta G_{\text{mix}}$  in three-component monolayers.

2. An original approach was established to quantify the apical and basolateral localization of hBest1 based on confocal microscopy data.

## VII. Publications related to the dissertation topic: 18

### With an impact factor: 16

1. **Jordan A. Doumanov**, Kirilka Mladenova, Vesselina Moskova-Doumanova, Tonya D. Andreeva, Svetla D. Petrova. Self-organization and surface properties of hBest1 in models of biological membranes. *Advances in Colloid and Interface Science*, accepted February 2022, (302)102619, **Q1**, **IF 15.19**, **Citations-1** <https://doi.org/10.1016/j.cis.2022.102619>
2. Pavel Videv; Kirilka Mladenova; Tonya D. Andreeva; Jong Hun Park; Veselina Moskova-Doumanova; Svetla D. Petrova; **Jordan A. Doumanov**; Cholesterol Alters the Phase Separation in Model Membranes Containing hBest1; 2022;

3. a) Erik Dimitrov, Natalia Toncheva-Moncheva, Pavel Bakardzhiev, Aleksander Forsys, **Jordan Doumanov**, Kirilka Mladenova, Svetla Petrova, Barbara Trzebicka and Stanislav Rangelov; Nucleic acid-based supramolecular structures: vesicular spherical nucleic acids from a non-phospholipid nucleolipid; *Nanoscale Advances*, August 2022, **Q1, IF 5.598, Citations-1**, 10.1039/d2na00527a
4. b) Erik Dimitrov, Natalia Toncheva-Moncheva, Pavel Bakardzhiev, Aleksander Forsys, **Jordan Doumanov**, Kirilka Mladenova, Svetla Petrova, Barbara Trzebicka and Stanislav Rangelov; Original Synthesis of a Nucleolipid for Preparation of Vesicular Spherical Nucleic Acids; *Nanomaterials* 2022, 12, 3645, **Q1, IF 5.719, Citations-1**, <https://doi.org/10.3390/nano12203645>
5. Pavel Videv, Nikola Mladenov, Tonya Andreeva, Kirilka Mladenova, Veselina Moskova-Doumanova, Georgi Nikolaev, Svetla D. Petrova, **Jordan A. Doumanov**, Condensing Effect of Cholesterol on hBest1/POPC and hBest1/SM Langmuir Monolayers; 2021, *Membranes*, Volume 11, Issue 1, 52, **Q2, IF 3.094, Citations-3**, 10.3390/membranes11010052
6. Mladenov, N (Mladenov, N.) Petrova, S (Petrova, S.) Andreeva, T (Andreeva, T.) Moskova-Doumanova, V (Moskova-Doumanova, V.) Videv, P (Videv, P.) Mladenova, K (Mladenova, K.) **Doumanov, J (Doumanov, J.)**, Effect of cholesterol on mixed hBest1/lipid monolayers, *FEBS OPEN BIO*, 2021, Volume 11, Page 224-224, Supplement 1, **Q2, IF 2.693**
7. Nikola Mladenov, Svetla D. Petrov, Kirilka Mladenov, Desislava Bozhinov, Veselina Moskova-Doumanov, Tanya Topouzova-Hristov, Pavel Videv, Ralitsa Veleva, Aneliya Kostadinov, Galya Staneva, Tonya D. Andreev, **Jordan A. Doumanov**, Miscibility of hBest1 and sphingomyelin in surface films – A prerequisite for interaction with membrane domains, 2020, *Colloids and Surfaces B: Biointerfaces*, 189, 110893, **Q1, IF 3.973**, 10.1016/j.colsurfb.2020.110893
8. Tonya D. Andreeva, Svetla D. Petrova, Kirilka Mladenova, Veselina Moskova-Doumanova, Tanya Topouzova-Hristova, Yulia Petseva, Nikola Mladenov, Konstantin Balashev, Zdravko Lalchev, **Jordan A. Doumanov**, Effects of Ca<sup>2+</sup>, Glu and GABA on hBest1 and composite hBest1/POPC surface films, *Colloids and Surfaces B: Biointerfaces*, 2018, 161, 192–199, **Q1, IF 4.295, Citations-3**, <https://doi.org/10.1016/j.colsurfb.2017.10.051>
9. Kirilka Mladenova, Svetla D. Petrova, Tonya D. Andreeva, Veselina Moskova-Doumanova, Tanya Topouzova-Hristova, Yuri Kalvachev, Konstantin Balashev, Shomi S. Bhattacharya, Christina Chakarova, Zdravko Lalchev, **Jordan A. Doumanov**, Effects of Ca<sup>2+</sup> ions on bestrophin-1 surface films, *Colloids and Surfaces B: Biointerfaces*, 2017, 149 (2017) 226–232, **Q1, IF 3.902, Citations-6**, <http://dx.doi.org/10.1016/j.colsurfb.2016.10.023>
10. a) Kirilka Mladenova, Svetla Petrova, Veselina Moskova-Doumanova, Tanya Topouzova-Hristova, Stoyanka Stoitsova, Irena Tabashka, Christina Chakarova, Zdravko Lalchev, **Jordan Doumanov**, Transepithelial resistance in human bestrophin-1 stably transfected Madin-Darby canine kidney cells, *Biotechnology and*

biotechnological equipment, Tome 29, Number 1, 2015, p. 101-104, ISSN (print):1310-2818, ISSN (online):1314-3530, **Q4, IF 0.622, Citations-1**, doi:10.1080/13102818.2014.988078

11. b) K. Mladenova, S. Petrova, T. Andreeva, V. Moskova-Doumanova, Z. Lalchev, **J. Doumanov**, Effect of Ca<sup>2+</sup> ions on Bestrophin-1 interaction with 1-palmitoyl-2-oleoyl-sn-glycero-3-phosphocholine in surface films, FEBS journal suppl., 2015, Volume 282, p. 319, Supplement 1, **Q1, IF 4.53**
12. Kirilka Mladenova, Svetla D. Petrova, Georgi As. Georgiev, Veselina Moskova-Doumanova, Zdravko Lalchev, **Jordan A. Doumanov**, Interaction of Bestrophin-1 with 1-palmitoyl-2-oleoyl-sn-glycero-3-phosphocholine (POPC) in surface films, Colloids and Surfaces B: Biointerfaces, 2014, ISSN 1873-4367, 122/ 432-438, **Q1, IF 4.287, Citations-9**, doi: 10.1016/j.colsurfb.2014.01.045
13. Veselina Moskova-Doumanova, Kirilka Mladenova, Svetla Petrova, Tanya Topouzova-Hristova, Christina Chakarova, Zdravko Lalchev, **Jordan Doumanov**, Amino acid exchange R25W affects proper cellular localization of Best1 protein in MDCKII cells, Comptes rendus de l'Academie bulgare des Sciences, 2014, Tome 67, Number 2, **Q3, IF 0.198**
14. **Jordan Doumanov**, Kirilka Mladenova, Radoslav Aleksandrov, Georgi Danovski, Svetla Petrova, Interactions of pharmacologically active snake venom sPLA2 with different cell lines, , Biotechnology and biotechnological equipment, Tome 28, Number 5, 2014, p.918-922, ISSN (print):1310-2818, ISSN (online):1314-3530, **Q4, IF 0.622, Citations-3**, doi: doi.org/10.1080/13102818.2014.965014
15. K. Mladenova, V. Moskova-Doumanova, I. Tabashka, S. Petrova, Z. Lalchev and **J. Doumanov**, Establishment and haracterization of stably transfected MDCK cell line, expressing hBest1 protein, Bulgarian Journal of Agricultural Science, 2013, 19 (2), 159–162, **Q3, IF 0.189**
16. **Doumanov JA**, Zeitz C, Dominguez Gimenez P, Audo I, Krishna A, Alfano G, Diaz ML, Moskova-Doumanova V, Lancelot ME, Sahel JA, Nandrot EF, Bhattacharya SS., Disease-causing mutations in BEST1 gene are associated with altered sorting of bestrophin-1 protein, Int J Mol Sci., 2013 Jul 22;14(7):15121-40, **Q2, IF 2.464, Citations-16**, doi: 10.3390/ijms140715121

**Total IF 62.303**

**Total number of citations - 44**

**Without impact factor: 2 бр.**

17. Pavel Videv, Kirilka Mladenova, Svetla Petrova, **Jordan Doumanov**, STRUCTURE AND FUNCTION OF hBEST1, EXPRESSED IN MDCK II CELLS, , Sofia University, “St. Kliment Ohridski”, Faculty of Biology, Department of Biochemistry, Bulgaria, 1164 Sofia, 8 Dragan Tzankov Blvd., 2019, p. 387-395, PKP-Print, <https://drive.google.com/file/d/1E-wzQ-k1L163yRieYFg8TI1j1mw0Hj5p/view?usp=sharing>, ISSN 1314-3425, регистрирана в НАЦИД

18. Kirilka Mladenova, Svetla Petrova, Veselina Moskova-Doumanova, Albena Jordanova, Tanya Topouzova-Hristova, Zdravko Lalchev and **Jordan Doumanov**, Characterization of morphology and growth rate of stably transfected MDCK cell line, expressing wild type of hBest1 protein, Science and technology, 2013, Volume III, Number 1, 32-36

## VIII. Participation in scientific forums

### National:

1. Pavel Videv, Jon Hun Park, Nikola Mladenov, Tonya Andreeva, Veselina Moskova-Doumanova, Kirilka Mladenova, Svetla Petrova, Jordan Doumanov, EFFECT OF CA<sup>2+</sup> ON COMPOSITE BESTROPHIN-1 LANGMUIR MONOLAYERS, XXXI МЕЖДУНАРОДНА ONLINE НАУЧНА КОНФЕРЕНЦИЯ, Шестдесет години СЪЮЗ НА УЧЕНИТЕ – СТАРА ЗАГОРА, 03-04 юни 2021 год
2. P. Videv, K. Mladenova, T. Andreeva, N. Mladenov, J. H. Park, V. Moskova-Doumanova, S. Petrova, J. Doumanov, MORPHOLOGY OF COMPOSITE HBEST1/POPC AND HBEST1/SPHINGOMYELIN MONOLAYERS, SCIENTIFIC CONFERENCE KLIMENT'S DAYS, 05/11-05/11, 2020, Sofia
3. Никола Младенов, Светла Петрова-Чанкова, Ралица Велева, Павел Видев, Кирилка Младенова, Йордан Думанов, РАЗПРЕДЕЛЕНИЕ НА HBEST1 В МЕМБРАННИ ДОМЕНИ ОТ ПЛАЗМЕНАТА МЕМБРАНА НА ЕУКАРИОТНИ КЛЕТКИ, Варненски медицински форум, т. 8, 2019, прил. 1, 13 - 15 септември 2019, Варна
4. Н. Младенов, С. Петрова, Т. Андреева, К. Младенова, В. Московка-Думанова, П. Видев, Т. Топузова-Христова, Й. Думанов; ЕФЕКТИ НА ТЕМПЕРАТУРАТА ВЪРХУ МОНОСЛОЕВЕ ОТ ЧОВЕШКИ БЕСТРОФИН-1; XXIX МЕЖДУНАРОДНА НАУЧНА КОНФЕРЕНЦИЯ, 6 – 7 юни 2019 година; Стара Загора
5. К. Младенова, С. Петрова, В. Московка-Думанова, Т. Топузова-Христова, П. Видев, Н. Младенов, Р. Велева, Т. Андреева, Й. Думанов; ВЛИЯНИЕ НА АТФ ВЪРХУ МОНОСЛОЕВЕ ОТ ЧОВЕШКИ БЕСТРОФИН-1; XXIX МЕЖДУНАРОДНА НАУЧНА КОНФЕРЕНЦИЯ, 6 – 7 юни 2019 година; Стара Загора
6. Nikola Mladenov, Svetla Petrova, Tonia Andreeva, Kirilka Mladenova, Desislava Vojinova, Ralitsa Veleva, Veselina Moskova-Doumanova, Pavel Videv, Yulia Petseva, Tanya Topouzova-Hristova, Jordan Doumanov, EFFECTS OF GLU AND GABA ON BEST1/SM MONOLAYERS, INTERNATIONAL SCIENTIFIC CONFERENCE "KLIMENT'S DAYS", 8-9 November 2018 Sofia, Faculty of Biology, SU

7. Nikola Mladenov, Kirilka Mladenova , Pavel Videv, Veselina Moskova-Doumanova, Tanya Topouzova-Hristova, Zdravko Lalchev, Tonya Andreeva, Svetla Petrova, Jordan Doumanov, TENSIMETRIC INVESTIGATIONS OF HBEST1 AND SM MONOLAYERS, YOUTH SCIENTIFIC CONFERENCE “KLIMENT’S DAYS”, 16-17 November 2017, Sofia, Faculty of Biology
8. N. J. Mladenov, S. D. Petrova-Chankova, T. D. Andreeva, K. S. Mladnova, T. I. Topouzova-Hristova, V. S. Moskova-Doumanova, Y. G. Petseva, Z. I. Lalchev, J. A. Doumanov, AFM and BAM investigations of hBest1 and sphingomyelin monolayers, Folia medica, 2017, vol. 59, suppl. 1
9. Н. Младенов , С. Петрова-Чанкова , Т. Андреева , К. Младенова , Т. Топузова-Христова , В. Москова-Думанова , Ю. Пецева, З. Лалчев , Й. Думанов , ЕФЕКТИ НА ГАВА ВЪРХУ МОНОСЛОЕВЕ ОТ ЧОВЕШКИ БЕСТРОФИН-1, XXVII МЕЖДУНАРОДНА НАУЧНА КОНФЕРЕНЦИЯ, ПОСВЕТЕНА НА 65 ГОДИНИ "МИНИ МАРИЦА - ИЗТОК", 1-2 юни 2017 година
10. Пленарен доклад, Assoc. prof. Jordan Doumanov PhD, Department of Biochemistry, Sofia University St. Kliment Ohridski, Cellular Polarity and Retinal Pathologies, Младежка научна конференция “Климентови дни” 17-18 ноември, 2016 г., София, Биологически факултет
11. K. MLADENOVA, S. PETROVA T. ANDREEVA, N. MLADENOV, V. MOSKOVA-DOUMANOVA, T. TOPOUZOVA-HRISTOVA, Y. PETSEVA, K. BALASHEV, Z. LALCHEV, J. DOUMANOV, VISUALIZATION OF HBEST-1 PROTEIN BY ATOMIC-FORCE MICROSCOPY, Постер M27, Младежка научна конференция “Климентови дни” 17-18 ноември, 2016 г., София, Биологически факултет
12. К. Младенова, С. Петрова, Т. Андреева, В. Москова-Думанова, Т. Топузова-Христова, Р. Велева, Е. Йоцова. Лалчев, Й. Думанов, ПРИЛОЖЕНИЕ НА АТОМНО-СИЛОВАТА МИКРОСКОПИЯ ПРИ ИЗСЛЕДВАНЕ НА ТРАНСМЕМБРАННИ БЕЛТЪЦИ, XXVI МЕЖДУНАРОДНА НАУЧНА КОНФЕРЕНЦИЯ, 2-3 Юни, 2016, Стара Загора
13. Kirilka Mladenova, Svetla Petrova, Tonya Andreeva, Ekaterina Yotsova, Veselina Moskova-Doumanova, Tanya Topouzova-Hristova, Zdravko Lalchev, Jordan Doumanov, Influence of  $\gamma$ -aminobutyric acid on Bestrophin-1 interaction with POPC in Langmuir monolayers, Младежка научна конференция “Климентови дни”, 18-20.11.2015, постер KD16, Биологически Факултет на СУ „Св Климент Охридски”
14. Kirilka Mladenova, Svetla Petrova, Tonya Andreeva, Ekaterina Yotsova, Veselina Moskova-Doumanova, Zdravko Lalchev, Jordan Doumanov, Influence of glutamate on Bestrophin-1 interaction with POPC in Langmuir-Blodgett films, Anniversary Conference of the Roumen Tsanev Institute of Molecular Biology, 5-6 October, 2015
15. Kirilka Mladenova, Svetla Petrova, Veselina Moskova-Doumanova, Tanya Topouzova-Hristova, Christina Chakarova, Zdravko Lalchev And Jordan

- Doumanov, (2013) Transepithelial resistance in human bestrophin-1 stably transfected MDCK cells, International Conference "Bioscience - development and new opportunities" - KLIMENT'S DAYS 2013, poster MB38, Sofia, Bulgaria
16. Jordan Doumanov, Virginia Doltchinkova, Kirilka Mladenova, Radoslav Aleksandrov, Georgi Danovski, Stoyan Chakarov, Svetla Petrova,(2013), Altered surface properties of MDCK-hBest1 cells treated with toxic sPLA2, International Conference "Bioscience - development and new opportunities" - KLIMENT'S DAYS 2013, poster MB36, Sofia, Bulgaria
  17. Kirilka Mladenova, Svetla Petrova, Veselina Moskova-Doumanova, Albena Jordanova, Tanya Topouzova-Hristova, Zdravko Lalchev and Jordan Doumanov, (2013), Characterization of morphology and growth of stably transfected MDCK cell line, expressing wild type of hBest1 protein, 23th International Scientific Conference, 6 - 7 June 2013, Stara Zagora, Bulgaria
  18. Kirilka Mladenova, Veselina Moskova-Doumanova, Petya Koleva, Tanya Hristova-Topouzova and Jordan Doumanov, (2013), Establishment of stably transfected MDCK cell line expressing wild type of hBest1 protein, Proceedings of the fourth workshop on experimental models and methods in biomedical research, p.153, 2013, Sofia, Bulgaria
  19. K. Mladenova, V. Moskova-Doumanova, I. Tabashka, S. Petrova, Z. Lalchev and J. Doumanov, (2012), Establishment and characterization of stably transfected MDCK cell line, expressing hBest1 protein, KLIMENT'S DAYS 2012, poster P43, Sofia, Bulgaria
  20. V. Moskova-Doumanova, J. Doumanov., (2012), Expression and localization of hBest1 in MDCK II cells, FEBS Advanced lecture course "Sofia school of protein science: structure and dynamics of biological macromolecules", 9-14 september 2012, p. 22, Sofia, Bulgaria
  21. Veselina Moskova-Doumanova, Kirilka Mladenova, Zdravko Lalchev, Jordan Doumanov, (2012), Are the RPE-derived cell lines RPE-1 and RPE-J appropriate model for investigation of cellular localization of Best1 protein, Third workshop on Experimental models and methods in Biomedical research, 23-25 April 2012, oral presentation A01, Sofia, Bulgaria.

#### **Abroad:**

22. V. Moskova-Doumanova, A. Krishna, E. Nandrot, P. Dominguez Gimenez, A. Jordanova, Z. Lalchev, SS. Bhattacharya, J. Doumanov, (2011), Investigation of cellular localization of the R25W Best1 mutant, , IVth International Congress of Molecular Medicine, 27-30.06.2011, poster 148, Istanbul, Turkey, In Vivo, vol.25, number 3, p. 524

**Successfully defended 4 diploma and 3 dissertation theses for the scientific and educational degree "Doctor" at the Department of "Biochemistry" on separate issues from the subject of the dissertation, Faculty of Biology, SU "St. Kliment Ohridski".**